



Monitoring sudden stratospheric warmings under climate change based on reanalysis data verified by radio occultation

Ying Li¹, Gottfried Kirchengast², Marc Schwaerz², Yunbin Yuan¹

¹ State Key Laboratory of Geodesy and Earth's Dynamics, Innovation Academy for Precision Measurement Science and Technology (APM), Chinese Academy of Sciences, Wuhan, 430071, China

² Wegener Center for Climate and Global Change (WEGC) and Institute of Physics, University of Graz, 8010 Graz, Austria

Correspondence to: Ying Li (lying@asch.whigg.ac.cn), Gottfried Kirchengast (gottfried.kirchengast@uni-graz.at)

Abstract. We develop a new approach to monitor Sudden Stratospheric Warming (SSW) events under climate change since 1980 based on reanalysis data, verified by radio occultation data. We construct gridded daily-mean temperature anomalies and employed the concept of Threshold Exceedance Areas (TEAs), the geographic areas wherein the anomalies exceed predefined thresholds (such as 30 K) to monitor the phenomena. We derived main-phase TEAs to monitor SSW warming on a daily basis and also a trailing-phase TEA to monitor potential upper stratospheric cooling in the wake of the warming phase. Based on the main-phase TEAs, three key metrics, including Main-Phase Strength (MPS), Duration (MPD) and Area (MPA), are estimated and used for the detection and classification of SSW events, enabling minor, major, and extreme event categories. An informative 42 winters' SSW climatology 1980-2020 was developed, including the three key metrics as well as onsets date, maximum-warming-anomaly location and strength and other valuable SSW characterization information. Detection and validation against previous studies underpins that the new method is robust for SSW detection and monitoring and that it can be applied to any quality-assured reanalysis and observational data that cover the polar region and winter timeframes of interest. Within the 42 winters, 40 SSW events were detected, yielding a frequency of about 0.95/year. In the 1990s, where recent studies showed gaps, we detected several events. About 95% of event onset dates occurred in deep winter (Dec-Jan-Feb timeframe; about 50% in January) and three quarters have their onset location over Northern Eurasia and the adjacent polar ocean. Regarding long-term change, we also found a statistically significant increase in the duration of SSW main-phase warmings, by about 4 days from the 1980s to the 2010s, raising the average duration by 40% from about 10 to 14 days and inducing an SSW strength increase by near 30 million km² days (about 30%) from about 105 to 135 million km² days. The results can be used as a reference for further long-term studies and be a valuable basis for studying SSW impacts and links to other weather and climate phenomena, such as changes in polar vortex dynamics and in mid-latitude extreme weather.



1 Introduction

30 Sudden Stratospheric Warming (SSW) describes an atmospheric variability phenomenon at daily-to-monthly scale where temperature in middle stratosphere (about 30 km or 10 hPa) increase rapidly (>30 to 40 K) within a couple of days in sub-polar and polar regions (McInturff et al., 1978; Butler et al., 2015; Baldwin et al., 2020). In extreme cases, SSW temperature anomalies can reach more than 70 K relative to the long-term mean. Many major SSWs occur accompanied by regular westerly winds reversed and/or polar vortex displaced or even split (Charlton and Polvani, 2007; Hu et al., 2015; Butler and Gerber, 2018). SSWs are generally understood to be caused by tropospheric planetary waves, which penetrate into the stratosphere, by the Quasi-Biennial Oscillation (QBO) and the Southern Oscillation (SO) in the tropics, which influence the stratospheric polar vortex, and also by solar radiation (McInturff et al., 1978; Thompson et al., 2002; Labizke and Kunze, 2009). SSWs usually occur in the polar regions of the northern hemisphere (beyond 60°N), while they rarely occur in the southern polar region due to less tropospheric planetary wave activity (Van Loon et al., 1973). We therefore focus on SSWs of northern hemisphere in this SSW-ensemble-based analysis over multiple decades since 1980.

SSWs are an important indicator of polar winter variability. They strongly interact with the troposphere (Hitchcock and Simpson, 2014; Lehtonen and Karpechko, 2016), mesosphere (Vignon and Mitchell, 2015; Singh and Pallamraju, 2015) as well as the upper atmosphere and ionosphere (Jonah et al., 2013; Kakoti et al., 2020) through atmospheric circulations and thermodynamics that mediate stratosphere-mesosphere-thermosphere couplings. The warming in the middle stratosphere will, on the one hand, propagate downwards to lower altitude levels and cause longer lasting warming in lower stratosphere (Hitchcock and Simpson, 2014). Some extreme events have impacts into deep troposphere and cause large area of blocking high pressure, and subsequently cause cold weather in northern Europe, eastern Asia and northern America regions (Cattiaux et al., 2010; Yu et al., 2015; Tyrllis et al., 2019; Hall et al., 2021). Some SSW events also cause the cooling of mesosphere and elevated stratopause (Holt et al., 2013; Vignon and Mitchell, 2015; Singh and Pallamraju, 2015). In the ionosphere, the distribution of electron density are found to be changed as a response to SSW (Nayak and Yigit, 2019; Kakoti et al., 2020). Due to atmospheric meridional circulation, the tropical stratosphere is found to be cooling at the same time as there is polar stratospheric warming (Yoshida and Yamazaki, 2011; Dhaka et al., 2015). Regarding atmospheric composition and chemistry, such as the distribution of ozone, water vapour and energetic particle precipitation, these are found to be changed as well (Kuttippurath and Nikulin, 2012; Ayarzagüena et al., 2013; Holt et al., 2013).

55 Given this variety of strong interactions of SSWs, it is important to accurately observe, detect, and monitor such events, including their possible transient changes under climate change. Accurate SSW observations require high quality data to be sufficiently dense in polar stratosphere. However, observations in these regions are notoriously sparse. Early studies used radiosonde or rocketsonde to observe SSWs. However, both datasets are generally land-limited and cannot provide high vertical resolution and high quality data throughout the lower, middle, and upper stratosphere. With the advent of satellite era in the 1970s, it is possible to put instruments, such as microwave limb sounders, infrared spectrometers and radiometers, on satellites in order to observe the atmosphere globally (e.g., Hitchcock et al., 2013; Noguchi et al., 2020). However,



satellite passive sounding data come in the form of radiances, which only allow coarse vertical resolution limiting the accurate conversion to altitude-resolved temperature or wind profiles, which are key variables for reliable SSW monitoring. With the advances of atmospheric data assimilation systems, reanalysis data have become quite a reliable data source for long-term atmospheric analyses, due to their advantages of regular sampled in space and time and capability to provide reasonably reliable data up to the stratopause (e.g., Charlton and Polvani, 2007; Yoshida and Yamazaki, 2011; Butler et al., 2017, 2018; Hersbach et al., 2020). However, reanalysis data may have inhomogeneities and irregularities in the long-term, due to episodic observation system updates and adding in a diversity of new streams of observation datasets over multi-decadal time ranges; they are not a direct long-term consistent observation of the atmosphere.

In addition to the sparsity of robust observation techniques, SSWs also have no community-agreed standard definition for reliable detection and monitoring. Butler et al. (2015) provided a detail overview on the history of various SSW definitions and calculated SSW frequency to cross-evaluate nine different definitions based on reanalyses data. Their results suggest that frequencies obtained using different definitions vary a lot, from about 0.46 to 0.81 events per year, and the onset (or maximum anomaly) dates of major SSWs for each definition may differ substantially as well. **Reasons of these discrepancies include both data and method reasons.** Regarding data aspects, reanalyses data, as stated above, may have inhomogeneities over time. Definitions based on one latitude or region are more sensitive to such variations than definitions based on larger domains (Butler et al., 2015). Regarding method aspects, the detailed implementation in selecting detection variable, latitude, altitude, thresholds and background climatology information can make the results quite different. These discrepancies of SSW definitions make statistical assessments of SSWs rather difficult. Furthermore, at the side of atmospheric physics and dynamics, the analysis of other weather and climate phenomena that relate to SSWs is also severely hindered if accurate SSW diagnostics and monitoring cannot be given.

~~Motivated by the aim~~ to help mitigate these current limitations, we here propose and apply a new method to monitor SSW events over the 1980 to 2021 northern hemisphere winter half-years, using Global Navigation Satellite System (GNSS) Radio Occultation (RO) data (Angerer et al., 2017) and ECMWF Reanalysis 5th generation (ERA5) data (Hersbach et al., 2020), developing a 42 years' SSW events tracking, and evaluating their characteristics.

GNSS RO is an atmospheric remote sensing technique to provide vertical atmospheric profiles, such as of temperature, density, and pressure (Kursinski et al., 1997; Kirchengast, 2004). RO data have distinctive advantages of high vertical resolution, high accuracy, long-term consistency, and global coverage (Anthes et al., 2011; Steiner et al., 2011). The vertical resolution of RO in the stratosphere is about 1 km, which is very high compared with other global observation techniques. Validation results against radiosonde and verification with (re)analysis data (that generally assimilate RO data) suggest that the data are of small discrepancy (< 2 K) in the upper troposphere and lower stratosphere (Scherllin-Pirscher et al., 2011a, b; Ladstätter et al., 2015; Steiner et al., 2020a, 2020b). RO data from different satellites can be combined without inter-calibration, which make them very suitable for climate-related studies (Foelsche et al., 2011; Angerer et al., 2017; Steiner et al., 2020a). Finally, since a multi-RO satellite observation record started in 2006 (Angerer et al., 2017), the geographic data coverage is sufficiently dense for monitoring and analysing regional-scale phenomena such as SSWs from that time onwards.



Complementary to reanalysis datasets, which also offer dense coverage, RO reprocessing datasets ~~hence~~ feature accurate and long-term stable observational records of climate benchmark quality (Steiner et al., 2020a), allowing for stable conditions for SSW monitoring over decades. Therefore, given the complementarity of these single-source long-term consistent benchmark observations to reanalyses (Bosilovich et al., 2013; Parker, 2016; Simmons et al., 2020; Hersbach et al., 2020), RO data are
100 ~~basically very suitable~~ for SSW studies.

An initial use of RO data for SSW study was by Klingler (2014) who was the first to use the data to examine the temperature changes during the 2009 SSW event. A couple of studies have also used RO data to analyse their impacts on gravity wave activity, the ionosphere, and also the tropical atmosphere (Yue et al. 2010, Lin et al. 2012, Dhaka et al., 2015). However, use for longer-term SSW detection and monitoring is a next step to be made. We have carried out an initial study (Li et al., 2021),
105 where we used RO data and ERA5 data to develop a new threshold-exceedance-area-based approach to monitor and characterize the strong and well-known 2009 SSW event. We revealed, in principle, high potential for the new method to be used for detection and monitoring of SSWs over multi-decadal timeframes as well.

In this study, building upon the initial Li et al. (2021) work, we apply the approach over 14 winters of RO data (2007 to 2020) and 42 ones (1980 to 2021) of ERA5 data, using the former reprocessing record to cross-verify the latter reanalysis dataset
110 for the purpose. We derive robust SSW characterization metrics, a new definition based on temperature field data, and apply the new method for SSW detection, classification, and monitoring, and to explore long-term changes in their characteristics under the recent climate change.

The paper is structured as follows. Section 2 briefly assesses current SSW detection methods and definitions and then summarizes the features of our new method. Section 3 introduces the data and methodology of our method and Section 4
115 presents and discusses the results. Finally, conclusions are given in Section 5.

2 Assessment of current definitions and the new method

2.1 Current definitions

A Sudden Stratospheric Warming (SSW) was first observed by Richard Scherhag using radiosonde measurements in Berlin, Germany, in January/February 1952 (Scherhag, 1952). He found an abrupt temperature increase in stratosphere. After about
120 a decade, the World Meteorological Organization (WMO) Commission for Atmospheric Sciences (CAS) developed an international SSW monitoring program called STRATALERT based on available radiosonde and rocketsonde observations (WMO/IQSY 1964). The WMO CAS suggested to provide an SSW warning, when a sudden and unusual increase in temperature at 30 km or above is detected.

~~With time ongoing and~~ after more events were observed, it was well recognized that many SSWs occurred along with wind reversals and/or polar vortex displacement or split (Johnson et al., 1969; Charlton and Polvani, 2007). Since the 1970s, many
125 studies combined temperature increase and wind reversals to detect SSWs, though detailed implementation and thresholds used are quite different (e.g., Schoeberl, 1978; Labitzke, 1981). An often-used definition at this stage was suggested by



McInturff et al. (1978), who proposed that a moderate-temperature anomaly of more than 25 K is regarded a minor event, while a stronger temperature increase jointly observed with wind reversal is regarded a major event.

130 Since wind reversal is one of the most important features of SSWs, many studies suggest to use wind reversal for detecting major SSW events (e.g., Charlton and Polvani, 2007; Hu et al., 2015; Butler et al., 2015, 2017; Butler and Gerber, 2018). One of the most often used definitions is the one from Charlton and Polvani (2007) (denoted as CP07 hereafter): a major SSW occurs, when the zonal mean zonal winds at 60 °N at the 10 hPa level become easterly during wintertime. In addition to wind reversal definitions, there are also studies that used vortex moment, another important characteristic of the warmings,

135 to detect SSW events (Seviour et al., 2013; Mitchell et al., 2013). Furthermore, polar-cap or zonal-mean stratospheric at 10 hPa geopotential height anomalies were used to detect SSW events (Baldwin and Thompson 2009; Gerber et al., 2010). Butler et al. (2015) tested the sensitivity of SSW detection results to nine definitions and found SSW frequencies obtained under these different definitions to vary from 0.46 to 0.81 events per year, and the onset dates also to vary substantially. There are several reasons of these discrepancies. First of all, while SSWs usually occur along with wind reversal or polar

140 vortex change, this is not always the case. Several studies detected significant stratospheric warming but did not simultaneously detect wind reversals at the commonly used 60 °N or 65 °N latitude. For example, Mitchell et al. (2013), who used vortex geometry for diagnosing SSW, found half of their events inconsistent with those obtained by CP07. Secondly, single-latitude and/or single-altitude definitions such as for wind reversal may miss some important SSWs that occurred primarily in other latitude-altitude domains (e.g., Manney et al., 2015; Singh et al., 2015). Thirdly, definitions can be quite

145 sensitive to background climatology and specific thresholds used, especially if based on broad polar cap-mean anomalies. Finally, current definitions either use zonal-mean or polar cap-mean results, which do not enable dynamical 3D tracking of such events. However, the dynamic location and strength information is rather important for studies on SSW's interactions with other phenomena, both regarding causes and impacts.

In view of the literature we surveyed and from our own initial study (Li et al., 2021), we suggest that a new standard SSW

150 monitoring method should best directly build upon the name-coining sudden stratospheric warming as such (i.e., be temperature-field-based), for directly quantifying the polar winter anomalous thermal variability as its primary fingerprint. Secondly, it should robustly detect and characterize SSW events, from minor to extreme ones, as a whole phenomenon, without being unduly sensitive to details. Thirdly, the method should be readily applicable to both observational and model data (as long as they are sampled sufficiently densely, preferably grid-based), and not need adjustment to any specific

155 suitable dataset (e.g., a particular reanalysis, atmospheric forecast, climate model simulation, or observational data record). Finally, upon detection, the SSW monitoring metrics should be informative on the duration, strength, and dynamic location of each SSW, in order to facilitate long-term change monitoring and effective use in cause and impact studies. Implementing these suggestions, we propose our new method and definitions in Section 2.2.



2.2 New method and its features

160 SSWs, as reflected by their name, were originally determined by their strong and quick temperature increase. Therefore, in
the method proposed here, we use temperature as the key variable for the diagnostics. Compared to wind- and polar vortex-
based definitions, temperature is a more accessible parameter that can be obtained from various observations. In addition,
temperature is a well-related parameter, when analyzing SSW relations to other phenomena in the troposphere as well as the
mesosphere and thermosphere/ionosphere. Many studies chose to use temperature solely, or combined it with wind-field
165 changes in studying impacts of SSWs (e.g., Zhou et al., 2002; Siskind et al., 2010; Manney et al., 2015; Jonah et al., 2013;
Kakoti et al., 2020; Singh and Pallamraju, 2015; Vignon and Mitchell, 2015). Also, further thermodynamic variables, in
particular air density and pressure, are often readily available for auxiliary co-information (Li et al., 2021).

Based on temperature changes, we designed the method to be fairly insensitive to temperature field details. Firstly, we use
robust stratospheric temperature anomaly profiles at any data location (such as a grid point) as the basis for expressing the
170 local warming; using an anomaly technique that has been proved useful and robust in diagnosing many other climate and
atmospheric change phenomena such as related to tropical cyclones (Biondi et al., 2015), atmospheric blocking (Brunner et
al., 2016) or thermal imprints of wildfires (Stocker et al., 2021). As described in detail by Li et al. (2021) and summarized in
Section 3 below, we then calculate vertical mean anomalies in selected stratospheric layers and categorize them into large-
scale grid cells covering the polar region, based on which we compute, on a daily basis throughout wintertime, temperature
175 threshold exceedance areas and related metrics, which serve as the basis for SSW detection and monitoring.

In establishing SSW climatologies (i.e., cataloguing SSW events over a multi-decadal period), previous studies generally do
only provide information about onset dates and vortex-split or displacement. In the climatology we build based on the new
method, we can provide SSW event onset date (of maximum middle stratosphere warming), duration, exceedance area, and
strength, as well as complementary day-by-day dynamic tracking of the center location, associated maximum warming, and
180 areal extent of the exceedance area. Furthermore, previous published climatologies reach to 2013 only and lack quality over
the 1990s decade, while we provide a climatology continuously extending from 1980 to 2021 and hence filling these gaps.

Compared to our initial method introduction and its careful evaluation in Li et al. (2021), which was based on the strong
2009 SSW event only, we focused and refined the diagnostics towards the metrics so that it now fully deploys for multi-
decadal detection, classification, and monitoring. The details on data and methodology are described next in Section 3.

185 3 Data and methodology

3.1 RO data

Since 2001, a continuous record of RO data is provided by GNSS RO missions, including the Challenging Mini-satellite
Payload mission (CHAMP; Wickert et al., 2001), followed by the Gravity Recovery and Climate Experiment (GRACE,
Wickert et al., 2005), the Constellation Observing System for Meteorology, Ionosphere, and Climate Experiment (GRACE;



190 Wickert et al., 2005), and the Constellation Observing System for Meteorology, Ionosphere, and Climate (COSMIC; Schreiner et al., 2007), the European Meteorological Operational satellites (MetOp; Luntama et al., 2008), the Chinese FengYun-3C operational satellite (Sun et al., 2018), and others. Since the launch of COSMIC near mid-2006, which was is a constellation of six satellites, there is sufficient coverage with RO event observations for regional-scale studies such as on SSWs. Therefore, in this study, we use the RO data record from the wintertime 2006/07 onwards.

195 We use the atmospheric profiles from the Wegener Center for Climate and Global Change (WEGC), processed by its Occultation Processing System version 5.6 (denoted as OPSv5.6 hereafter). Several studies that introduced, validated and evaluated the OPSv5.6 record, showed that these data are of high quality (e.g., Ladstätter et al., 2015; Angerer et al., 2017; Scherllin-Pirscher et al., 2017; Steiner et al., 2020a; Schwärz et al., 2021). A detailed discussion of quality aspects is provided by Angerer et al. (2017). Based on the record available to end 2020, we use RO data from the winter seasons W06-
200 07 until W19-20, which are 14 winters (“W”) in total, which we define to comprise the extended-winter season from November to March (hence, for example, “W06-07” contains the November 2006 to March 2007 timeframe). We use the OPSv5.6 multi-satellite data from COSMIC, CHAMP, GRACE, MetOp, SAC-C, in the form as available from the WEGC dataset (Schwärz et al., 2021).

3.2 ECMWF Reanalysis 5 (ERA5) data

205 ERA5 is the fifth-generation ECMWF atmospheric reanalysis of the global weather and climate (Hersbach et al., 2019, 2020; Simmons et al., 2020). It was produced for the European Copernicus Climate Change Service (C3S) by ECMWF and replaces the ERA-Interim reanalysis (Dee et al., 2011), which stopped being produced by August 2019. ERA5 combines vast amounts of historical observations into global atmospheric gridded field estimates, using ECMWF’s modeling and data
210 assimilation system. The basic resolution of ERA5 is about 30 km horizontal resolution and 137 vertical levels from the surface up to an altitude of about 80 km. Here we use quality-assured ERA5 datasets, that are provided from 1979 onwards, over the 42 winters from 1979/80 (W79-80) to 2020/21 (W20-21), fully encompassing also the RO data period.

ERA5 data are used jointly with RO data for two purposes. Firstly, they are used as part of cross-checking the new method, to make sure that the method can be applied to both RO and reanalysis data. Secondly, since dense RO observations are only available from the year of 2006 onwards, we need to have reanalysis data, which provide much longer data records, to fully
215 explore our method and to develop a long-term SSW climatological record. We use then on a 2.5° latitude \times 2.5° longitude grid, to provide an adequate resolution that also roughly matches the RO horizontal resolution of about 300 km (eg. Kursinski et al. 1997; Anthes et al. 2008). In the vertical, we use the model-level resolution (137 levels), which is sufficiently dense for our stratospheric altitude range over 20 to 50 km. Temporal resolution used is 6 hours (four time layers per day, at 00, 06, 12 and
220 18 UTC), following the experience of many previous studies that intercompared and/or jointly used atmospheric (re)analysis and RO data (e.g., Gobiet et al., 2007; Scherllin-Pirscher et al., 2011; Angerer et al., 2017; Steiner et al., 2020a; Li et al., 2021).



Figure 1 illustrates characteristics of the RO and ERA5 profile datasets as relevant for the present SSW study, including on the daily number of events available (Fig. 1a) and for exemplary days during SSW events (Fig. 1b-d, see caption for details). Evidently RO observational atmospheric profile data are comparatively sparse over the (northern high-latitude) region of interest, while ERA5 as a gridded dataset regularly provides its profiles at each and every of its grid cells without sparsity. Hence, while the number of RO profiles is of the order of several hundred per day, the ones of ERA5 amount to near 10000 per day. Furthermore, as Figure 1b-d shows, the spatial distribution of ERA5 data is regular-on-grid, while RO events occur with reasonable overall coverage but irregular sampling in detail. A few exemplary events (“Event1” to “Event3”) are highlighted, against the back-plot of illustrated SSW temperature anomalies over the polar region, in order to use them next to explain the methodology.

3.3 Methodology

Since we recently provided a detailed basic introduction of the new SSW monitoring approach in Li et al. (2021) and discussed main overall features in Sect. 2.2 above already, we restrict to a brief summary here, supported by concise tabular information and focusing on updates and refinements since that introduction, which provides further technical details. Table 1, which is a condensed and refined update of Table 1 in Li et al. (2021), summarizes the basic parameters and features of the method, from definition of the temperature anomalies and the related daily threshold exceedance areas (TEAs) in three characteristic stratospheric layers (lines (1)-(4)) via the anomaly-maximum value and location (lines (5)-(6)) to the four derived TEA key variables during SSW events (lines (7)-(10) that monitor and characterize the different SSW phases.

Figure 2 graphically illustrates this construction of the anomalies and variables by way of the three example RO events indicated in Figure 1 as well as correspondingly for three ERA5 profiles from adjacent grid points. It can be seen that RO and ERA5 profiles are overall similar, with the latter profiles somewhat smoother in their resolution of vertical variability. Deviations of temperature and corresponding climatological profiles are smallest for Event1 that is located in a non-warming area (cf. Fig. 1b). Event2, and Event3 that are most affected, show larger deviations and anomalies than Event1 since these are located in the warming area of the SSW (cf. Figs 1b, 1d). Largest anomalies for the latter two events are found in mid-stratosphere layer (30-35 km), with values is about 45 K and 60 K, respectively. Maximum values in the other altitude layers are smaller. In this way, these few examples are consistent with the broader and long-term picture over many SSW events (see Sect. 4 below), which show the SSW warming to be strongest in the middle stratosphere (about 30 to 40 km).

While Li et al. (2021) introduced and tested the approach based on the single 2009 SSW event, we here made sure for long-term application that the four SSW TEA key variables are captured and exploited in a way so that they reliably detect and quantify actual SSW warmings, and cooling in the trailing phase if it occurs, among the on-going weaker and more “random” polar variability due to other driving factors. The rightmost column of Table 1 (lines (7)-(10) therein) summarizes the criteria that we chose after careful testing and sensitivity studies both with the RO and ERA5 data. Based on these well-selected TEA key variables and the auxiliary variables on maximum-values and locations, all prepared at daily sampling, we could



255 finally define the fundamental metrics and criteria that we use for the detection, classification and further qualification of
SSWs. These are summarized in Table 2, including brief explanations (rightmost column therein).

260 Extensive robustness and sensitivity testing provided us with due evidence and confidence that these characteristics,
effectively constructed from the dynamic temperature anomaly field as perturbed by the SSW, should enable a new level of
quality and quantitative insight into SSWs also in the long-term, completing the methodology from our initial Li et al. (2021)
single-event study. We hence applied the new method with the parameters and definitions summarized in Table 2 to the
complete RO and ERA5 datasets and discuss the results below.

4. SSW detection and monitoring results

4.1 Polar cap mean anomalies overview

265 Figure 3 illustrates RO (Fig. 3a) and ERA5 (Fig. 3b) polar cap (60 °N – 90 °N) daily mean temperature anomalies over the 15
winters period from W06-07 to W20-21, where both datasets overlap for 14 winters and where RO data can hence be used to
cross-verify ERA5 data. RO and ERA5 polar cap results appear rather similar, with anomalies from ERA5 data typically
about 5 K (occasionally up to 10 K) larger than RO data above 35 km. These differences can mainly be attributed to the
denser sampling of ERA5, leading to somewhat less spatial smoothing. In general, the overall closely similar results of these
independently produced and quite differently-sampled datasets (for detailed discussion see Li et al., 2021) lend confidence
that we may use ERA5 data for the inspection of the multi-decadal time period from 1980 onwards.

270 Figure 4 shows the complementary back-extended polar cap temperature anomalies of ERA5 for the 27 winter periods
W79-80 to W05-06. The results are overall similar with Figure 3 and both together provide a neat first overview on which
winter seasons hosted potentially strong SSWs (e.g., W84-85, W03-04, W18-19) and which appear comparatively quiet,
including with not relevant sign of SSWs (e.g., W81-82, W93-94, W10-12). It also appears to be a very salient feature
already in this polar cap-mean inspection that strong SSW events often are entailed by a distinct upper stratospheric cooling,
275 which is hence reflected in our metrics definitions (see Table 2, lines (6)-(8)). Another interesting feature hinted here already
is that in the 1990s, where existing SSW climatologies detect very few events (e.g., Charlton and Polvani., 2007; Hu et al.,
2015; Butler and Gerber., 2018), we do detect several reasonably strong SSWs that classify as major events (more details in
Sect. 4.4).

280 Figures 3 and 4 also show that some distinct temperature anomalies are found in almost every winter in one or another form,
which underlines the fact that the polar stratosphere is quite variable in winter. Regarding SSWs, some winters signal one
strong warming, while some others show multiple moderately strong or minor warmings. Strong warming propagates to lower
altitude levels and also cause longer-lasting warmings, and as noted above may be entailed by distinct cooling (such as in the
most recent decade W12-13 and W18-19). A final observation from this basic synoptic view is that the altitude range of
maximum warming varies somewhat from event to event. For example, the W11-12 warming is found-largest at about 35 to
285 40 km, while the W17-18 warming exhibits its largest anomalies at about 25 to 30 km. Our definition of main phase,



combining middle and lower stratospheric TEA diagnostics (see Table 1, line (9)), robustly captures such different specific event dynamics.

4.2 SSW threshold-exceedance-area representative results

Figure 5 shows spatial contour maps of typical daily temperature anomalies across the temporal evolution (top to bottom) of three representative SSW events of increasing strength (left to right; those already used for back-plot in Fig.1). Evidently, both the temperature anomalies' magnitude and warming area increase from minor to extreme event, which is in particular visible in the mid-stratosphere temperature anomaly on the event onset date (second row). Complementary to this, the snapshot day shown from the trailing phase (four weeks after onset date, bottom row) highlights that the extreme event (right) exhibit a very distinct upper stratosphere cooling anomaly, exceeding -40 K in a TEA of about 10 million km^2 size.

Following this representative spatial view on individual daily TEAs, from both warming and cooling anomalies, Fig.6 illustrates for the same three events (left to right) how our method leads from TEA timeseries in the three stratospheric layers (first three rows) to the TEA key variables (fourth row, above polar-map plots) from which finally the SSW metrics for the overall event characterization according to Table 2 are derived.

Daily TEA values over positive thresholds quantify the size of exceedance areas of warming while those over negative thresholds diagnose the exceedance areas of cooling. It can be seen, for example, that MSTA-TEAs over positive thresholds of all events increase rapidly to maximum and then quickly decrease, indicating the typical sudden warming of the primary phase. LSTA-TEAs over positive thresholds are overall of smaller magnitude but longer duration, and with maxima delayed against MSTA-TEAs, from the SSW downward propagation. Regarding event strength, while MSTA-TEAs >30 K of major and extreme events are relatively similar, the duration of the extreme event is longer than for the major event. The USTA-TEA timeseries of the extreme event shows the distinct several-weeks-long cooling behavior in the trailing phase.

The TEA key variables (Fig. 6j to 6l) capture the essential daily TEA information per SSW event, in the form summarized in lines (7)-(10) of Table 1, as the basis for the three key metrics per event according to lines (1)-(3) of Table 2, the quantified values of which are shown in the panel legends. As already indicated by the polar-cap-mean view in Figs 3 and 4, it is well seen here that the ERA5 TEAs (heavy lines) are generally higher than from the RO data (thin lines), which in particular applies for the trailing-phase cooling of the extreme event (Fig. 6l) in the upper stratosphere, where the sparser sampling by RO events leads to the relatively largest difference. In terms of magnitudes, it is clearly visible from the values that the MPS, MPD and MPA metrics reach that the event strength substantially grows from minor to extreme events (see also the strength class definitions based on the MPS in line (5) of Table 2).

The polar-map plots of Figure 6 (bottom row) finally illustrate the dynamic event tracking information of the SSW-PP-TEA, SSW-SP-TEA and SSW-TP-TEA timeseries for the three representative events. This view enables to see the geographic trajectory of the daily anomaly center location (maximum-value location, cf. line (6) of Table 1) together with an indication of the anomaly magnitude (color of corresponding TEA thresholds). This type of plots helps the detailed diagnostics and characterization of any specific event as introduced in Sect. 2 above (for details see also Li et al., 2021).



4.3 SSW detection and metrics-tracking results

320 Figures 7 and 8 employ the view introduced in Fig. 6j-6l to display the TEA diagnostics and MPS/MPD/MPA metrics results for all SSWs detected over the full multi-decadal period from 1980 to 2021 (Fig. 7 for the recent winters since 2001/02 and Fig. 8 for those before, up to 2000/01). Figure 7 shows that one or two SSWs have occurred during almost every winter (except in W04-05 and W10-11), while Fig. 8 indicates that there have been somewhat more SSW-quiet winters in the two decades before.

325 The strongest event during the entire period is the one in W08-09, with a main-phase strength (MPS) of over 360 million km^2 days for the ERA5 data (330 million based on the cross-verifying RO data). The second strongest event is the one of W18-19, where the MPS from ERA5 exceeded 290 million km^2 days. Additionally, the winters W01-02, W12-13 and W17-18, as well as the winters W84-85, W87-88, and W88-89 in the 1980s, hosted extreme events exceeding our classification threshold of $180 \times 10^6 \text{ km}^2$ days. Half of these eight extreme events also are seen to have caused a strong upper
330 stratospheric cooling during the trailing phase that lasted for more than a month.

In addition, several major events occurred (e.g., W02-03, W03-04, W05-06), with the MPS of such events varying from 90 to $180 \times 10^6 \text{ km}^2$ days as defined in Table 2. Also two of the major events caused a long-lasting upper stratospheric cooling in the trailing phase (in W03-04 and W05-06), which is an exception for these events, however. Together with these major events also a range of minor events were detected and diagnosed, exhibiting an MPS smaller than $90 \times 10^6 \text{ km}^2$ days. Based on
335 these long-term SSW tracking results shown in Figs 7 and 8, we are now prepared to collect and analyze the long-term results in a more climatological-statistical manner, including inspection for possible long-term transient changes in the record.

4.4 SSW climatology and monitoring under climate change

Table 3 provides a climatological summary of the ERA5-based results for all SSW events detected during the entire 42-years
340 period, listing for each event the main characteristics as defined by Table 2 and intercomparing the onset date to the onset dates found by the Butler and Gerber (2018) (BG18) work that extended to the year 2013. The latter intercomparison reveals that a range of minor and major events was not part of the BG18 list, while several are part of that list and not detected here. In general, the onset dates detected by the new method introduced here are consistent with those in the BG18 climatology, with coincidence of the dates commonly within ± 1 day.

345 As a complement, Table 4 shows the corresponding onset dates and key metrics as obtained from the RO data, which indicates that three minor events (in W07-08 and W19-20) were not making the detection threshold for this dataset though they were detected based on the ERA5 data. One of the two of W07-08, which overlaps with the BG18 data record, also was not detected by the BG18 work.

In terms of count statistics, we detected 40 events in the 42 winters, corresponding to a frequency of 0.95/year. Hence,
350 compared to the frequency estimate of 0.6/year provided by the BG18 definition, the new approach detects about 35% more



events, close to the frequency estimate of 0.9/year by McInturff (1978). In general, the high consistency of onset dates with the BG18 definition provides evidence that our new temperature-anomalies-based method is robust in detecting SSW events and that the warming anomalies are strongly related to wind reversals during SSWs. For those events detected by the BG18 definition but not by our method (e.g., the W06-07 event in February 2007), we do find minor warmings signaled also in our
355 TEA diagnostics, but they do not exceed thresholds long enough (at least one week) for detection according to Table 2.

For the higher number of events that we detected, but which are not detected by the BG18 definition, the main reason is that detection based on single altitude and latitude miss events occurred in other domain. Related to altitude, we found that a number of events occurred at levels higher than 10hPa and therefore such events were not detected by the BG18 definition (e.g., in W92-93 and W00-01). In W07-08, we basically found four warmings (as can be seen in Fig.3), of which two
360 satisfied our detection criterion, which is in line with Singh et al. (2015), who also found four warmings based on a temperature increase definition. Related to latitude, Hu et al. (2015) used a wind reversal definition at 65 °N, detecting an event on 26 January 2010, which is close to our onset date of 29 January 2010 rather than the BG18 date of 9 February 2010. This indicates that selection of a specific latitude for detection also can hinder reliable detection.

Furthermore, our detection of a number of events in the 1990s, while BG18 detect only one in W98-99, is mainly because a
365 significant amount of radiosonde stations ceased operations and the availability of wind measurements to the BG18 study was degraded. Our method, based on temperature data records (here primarily from ERA5, verified by RO data) is robust against such observation network changes and, in addition, temperature is also an easily available variable, including in form of multi-decadal records with reasonable long-term stability.

Figure 9 finally depicts summary statistics on the long-term results along various perspectives of interest (see the caption and
370 the respective panel titles for explanation of the various panels), in most cases (Fig. 9a-9d) visualizing also the strength class of the events according to the overarching MPS metric (by orange, red, dark-red color). While as a time series the MPS appears widely variable (Fig. 9a), the inspection of its component metrics MPD and MPA reveals that the former (the duration) most clearly drives the strength (Fig. 9b, upper left subpanel) and that a salient trail-cooling phase, indicated by the TPD and TPA auxiliary metrics, is dominated by some of the strongest events (Fig. 9b, lower subpanels). Furthermore,
375 almost all SSW onsets (95%) are found within the deep winter (i.e., the Dec-Jan-Feb timeframe, with about half in January; Fig. 9c) and more than three-quarters are found to have their onset location over northern Eurasia and the adjacent polar ocean (Fig. 9d).

Visually spotting a long-term “tendency” for perhaps some strength intensification, in Figs. 9a, b and the numbers of Table 3,
we also quantitatively inspected for long-term trends in MPS, MPD, and MPA, based on decadal-mean values over 1984 to
380 2016 center years (Fig. 9e; events allocated to a year based on their onset month; decadal means are 10-yr-aggregated values over center-yr-4 yrs to center-yr + 5 yrs divided by 10 yrs; cross-check to a simple averaging over the events in any 10-yr-window led to similar results but with somewhat more variability due to the sometimes small event count per decade). Using linear fitting (ordinary-least-squares trend fit, including uncertainty estimation for the trend rate accounting for reduced degrees-of-freedom due to autocorrelation and for small-sample t-distribution statistics; Santer et al., 2020; Loeb et al., 2022),



385 we indeed found a statistically significant positive trend in the MPS, with a best-estimate strength intensification by 9.3 million km² days per decade (95% significance level; Fig. 9e, left subpanel), which is driven by a highly significant increase in the MPD by about 1.3 days/decade (99% significance level; Fig. 9e, middle subpanel).

This implies an increase in the duration of SSW main-phase warmings by about 4 days from the 1980s to the 2010s, raising the average duration by 40% from about 10 to 14 days and inducing an SSW strength increase by near 30 million km² days (about 30%) from about 105 to 135 km² days. No significant trend was found in the MPA (Fig. 9e, right subpanel) as well as the associated threshold exceedance magnitude (the average warming strength of the main-phase temperature anomaly above threshold, as indicated by the Max ΔT threshold exceedance), for which sensitivity testing confirmed that it is well correlated with the MPA (not shown). We also find an increasing trend in the number of major and extreme SSW events, by about 0.4 events per decade (near 90% significance level); an analysis for which the time series is still quite short, however, and which depends for the minor event counts somewhat on the threshold definition for their detection.

While a detailed interpretation and further study of the possible causes of this increase in warming duration, including cross-comparison with other temperature field datasets beyond ERA5, is beyond the scope of this study that focuses on introducing the new monitoring method and related SSW climate data record, we speculate that it may be related to changes in the polar vortex dynamics over the recent decades that have led to transient change in prevalent vortex patterns, partly induced by anthropogenic climate change effects in the polar region (e.g., Kretschmer et al., 2018a;b). Since the MPS metric can be interpreted as an anomalous heat energy content contained in the exceedance warming of an SSW event (similar to the threshold exceedance metric of cooling degree days in the analysis of energy demand during hot days or even heat extremes; Forster et al., 2021), the estimated increase by about 30% since the 1980s corresponds to substantially more energy stored in and released by recent SSW events.

405 5 Conclusions

In this study we introduced and applied a new method for long-term monitoring of Sudden Stratospheric Warming (SSW) events based on metrics derived from daily stratospheric temperature anomaly threshold exceedance area data, refining upon the approach introduced in Li et al. (2021), which was based on the well-known 2009 SSW event only. We applied the new method over 1980 to 2021, including 14 winters using radio occultation (RO) data for verification (2006–2020), and all 42 winters within 1980–2021 from using ERA5 reanalysis data. Robust SSW characterization metrics including Main-Phase Duration (MPD), Area (MPA), and Strength (MPS) are derived, together with further auxiliary diagnostics.

Using these metrics, we proposed a new definition for SSW event detection and classification as well as explored multi-decadal changes in their characteristics under the recent climate change. According to MPS, SSWs are classified as minor, major, and extreme events. We also provide an informative SSW climatology over the four decades, recording valuable SSW event characterization information, including onset date, strength, duration, exceedance area, and type of event (minor, major, or extreme), complemented by the maximum-warming-anomaly geographic location and its associated maximum warming.



In addition, event trailing-phase metrics as well as day-by-day dynamic tracking of the warming-anomaly center location and associated maximum warming and of the areal extent of the exceedance area are available.

420 Detection results using RO and ERA5 are overall similar, suggesting that the new method can be applied using both RO and ERA5 data as well as any other quality-assured observational or reanalysis temperature (field) data covering the polar region and winter timeframes of interest. Comparison between our climatology with that from the recent BG18 climatology (Butler and Gerber, 2018) reveals that a number of minor and major events was not part of the BG18 study, while several are part of that one and not detected here. The coincidence of the onset dates of jointly detected events is commonly within ± 1 day, suggesting high detection consistency of the different methods and cross-verifying that our new method is robust.

425 In terms of event count statistics, we detected 40 events in the 42 winters, corresponding to an estimated event frequency of 0.95/year. Hence, compared to the frequency estimate of 0.6/year provided by the BG18 study, the new approach detects about 35% more events, close to the event frequency estimate of 0.9/year by McInturff (1978). Within the 1990s, where the BG18 study detected only two in W98-99, we detected a number of events. We also found that a salient upper stratospheric trailing-phase cooling occurs in the wake of the main warming phase for most, though not all, of the strongest events.
430 Regarding temporal and spatial occurrence, we found about 95% of the SSW onset dates in deep winter (i.e., Dec-Jan-Feb timeframe; about 50% in January) and more than three quarters of the associated onset locations over Northern Eurasia and the adjacent polar ocean.

Regarding long-term changes, using linear-trend fitting and statistical evaluation, we found a statistically significant positive trend in the MPS metric, with a best-estimate strength intensification by 9.3 million km² days per decade, which is driven by
435 a highly significant increase in the MPD by about 1.3 days/decade. This implies an increase in the duration of SSW main-phase warmings by about 4 days from the 1980s to the 2010s, raising the average duration by 40% from about 10 to 14 days and inducing an SSW strength increase by near 30 million km² days (about 30%) from about 105 to 135 million km² days. Since the MPS metric can be interpreted as an anomalous heat energy content contained in the exceedance warming of an event, such an increase by about 30% corresponds to substantially more energy stored in and released by recent SSW events.
440 No significant trend was found in the MPA as well as the associated threshold exceedance warming magnitude.

It is hoped that the results of this study can be used as a reference for further complementary long-term studies and, in particular, also be a basis for SSW impact studies related to other weather and climate phenomena linked to SSWs, such as changes in polar vortex dynamics and implications to mid-latitude extreme weather, among others. Follow-on work will further investigate the SSW's long-term evolution over the recent decades and the causes of the evidenced trends. We also
445 intend to investigate whether and how SSW events occurring in different regions have impacts on near-surface weather over middle latitudinal regions of the northern hemisphere.

Code availability. The code used to produce the results of this study is available from the first author (Y. L.) upon qualified request.

450



455

Data availability. The (numeric) data underlying the results of this study are available from the first author (Y. L.) upon qualified request. The ERA5 reanalysis data are available at full resolution via ECWMF's Mars archive (registered member state users) and publicly through the Copernicus Climate Change Services (C3S) via <https://cds.climate.copernicus.eu/>. The OPSv5.6 RO data of WEGC are publicly available via <https://doi.org/10.25364/WEGC/OPS5.6:2020.1>.

460

Author contributions. Ying Li implemented and refined the new method, performed the analysis, produced the figures, and wrote the initial draft of the manuscript. Gottfried Kirchengast conceived the method and served as primary coauthor, providing advice and guidance on all aspects of the design, analysis, and figure production, and significantly contributed to writing the manuscript. Marc Schwärz supported the setup and advancements of the OPS analysis system and provided input data as well as algorithms. Yunbin Yuan advised on analysis and algorithm comparisons. All authors commented on and agreed to the final submitted manuscript.

Competing interests. The authors declare that they have no conflict of interest.

465

Acknowledgements. We acknowledge ECMWF (Reading, UK) for providing access to their analysis and forecast data and the RO team at WEGC (Graz, Austria) for the preparation of the OPSv5.6 RO data; we specifically acknowledge Florian Ladstätter for supporting RO climatology provision and advising on its characteristics as well as on results interpretation. The research at the APM (Wuhan, China) was funded by the Strategic Priority Research Program of Chinese Academy of Sciences (Grant No. XDA17010304) and the Chinese Natural Sciences Foundation (grant no. 41874040). At WEGC, the work was supported by the Aeronautics and Space Agency of the Austrian Research Promotion Agency (FFG-ALR) under the Austrian Space Applications Programme (ASAP) projects ATROMSAF1 and ATROMSAF2 (proj.no. 859771 and 873696) funded by the Ministry for Climate, Environment, Energy, Mobility, Innovation, and Technology (BMK).

470

References

Angerer, B., Ladstätter, F., Scherllin-Pirscher, B., Schwärz, M., and Kirchengast, G.: Quality aspects of the Wegener Center multi-satellite GPS radio occultation record OPSv5.6, *Atmos. Meas. Tech.*, 10(12), 4845–4863, <https://doi.org/10.5194/amt-10-4845-2017>, 2017.

475

Anthes, R. A.: Exploring Earth's atmosphere with radio occultation: contributions to weather, climate and space weather, *Atmos. Meas. Tech.*, 4, 1077–1103, <https://doi.org/10.5194/amt-4-1077-2011>, 2011.

480

Ayarzagüena, B., Langematz, U., Meul, S., Oberländer, S., Abalichin, J., and Kubin, A.: The role of climate change and ozone recovery for the future timing of major stratospheric warmings, *Geophys. Res. Lett.*, 40, 2460–2465, <https://doi.org/10.1002/grl.50477>, 2013.



- Baldwin, M. P., Ayarzagüena, B., Birner, T., Butchart, N., Butler, A. H., Charlton-Perez, A. J., Domeisen, D.I.V., Garfinkel, C. I., Garny, H., Gerber, E. P., Hegglin, M. I., Langematz, U., and Pedatella, M.: Sudden stratospheric warmings. *Reviews of Geophysics.*, 59, <https://doi.org/10.1029/2020RG000708>, 2020.
- 485 Baldwin, M. P. and Thompson, D. W. J.: A critical comparison of stratosphere–troposphere coupling indices, *Quart. J. Roy. Meteor. Soc.*, 135, 1661–1672, <https://doi.org/10.1002/qj.479>, 2009.
- Biondi, R., Steiner, A. K., Kirchengast, G., and Rieckh, T.: Characterization of thermal structure and conditions for overshooting of tropical and extratropical cyclones with GPS radio occultation, *Atmos. Chem. Phys.*, 15, 5181–5193, <https://doi.org/10.5194/acp-15-5181-2015>, 2015.
- 490 Bosilovich M.G., Kennedy J., Dee D., Allan R., and O’Neill A.: On the Reprocessing and Reanalysis of Observations for Climate in *Climate Science for Serving Society*, edited by: Asrar, G. and Hurrell, J., Springer, Dordrecht, https://doi.org/10.1007/978-94-007-6692-1_3, 2013.
- Brunner, L., Steiner, A.K., Scherllin-Pirscher, B., and Jury, M.W.: Exploring atmospheric blocking with GPS radio occultation observations, *Atmos. Chem. Phys.*, 16, 4593–4604, <https://doi.org/10.5194/acp-16-4593-2016>, 2016.
- 495 Butler, A. H., Sjöberg, J. P., Seidel, D. J., and Rosenlof, K. H.: A sudden stratospheric warming compendium, *Earth Syst. Sci. Data*, 9, 63–76, <https://doi.org/10.5194/essd-9-63-2017>, 2017.
- Butler, A. H. and Gerber, E. P.: Optimizing the definition of a sudden stratospheric warming, *J. Climate.*, 31, 2337–2344, <https://doi.org/10.1175/JCLI-D-17-0648.1>, 2018.
- Butler, A. H., Seidel, D. J., Hardiman, S. C., Butchart, N., Birner, T., and Match, A.: Defining sudden stratospheric warmings, *B. Am. Meteor. Soc.*, 96, 1913–1928, <https://doi.org/10.1175/BAMS-D-13-00173.1>, 2015.
- 500 Cattiaux, J. R., Vautard, R., Cassou, C., Yiou, P., and Codron, F.: Winter 2010 in Europe: a cold extreme in a warming climate, *Geophys. Res. Lett.*, 37, 114–122, <https://doi.org/10.1029/2010GL044613>, 2010.
- Charlton, A. J. and Polvani, L. M.: A new look at stratospheric sudden warmings: Part I: Climatology and modeling benchmarks, *J. Climate.*, 20, 449–469, <https://doi.org/10.1175/JCLI3996.1>, 2007.
- 505 Dee, D. P., Uppala, S. M., Simmons, A. J., Berrisford, P., Poli, P., Kobayashi, S., Andrae, U., Balmaseda, M. A., Balsamo, G., Bauer, P., Bechtold, P., Beljaars, A. C. M., van de Berg, L., Bidlot, J., Bormann, N., Delsol, C., Dragani, R., Fuentes, M., Geer, A. J., Haimberger, L., Healy, S. B., Hersbach, H., Hólm, E. V., Isaksena, L., Kållberg, P., Köhler, M., Matricardi, M., McNally, A. P., Monge-Sanz, B. M., Morcrette, J.-J., Park, B.-K., Peubey, C., de Rosnay, P., Tavolato, C., Thépaut J.-N., and Vitart, F.: The ERA-Interim reanalysis: Configuration and performance of the data assimilation system, *Q.J.R.Meteorol.Soc.*, 137, 553–597, <https://doi.org/10.1002/qj.828>, 2011.
- 510 Dhaka, S. K., Kumar, V., Choudhary, R. K., Ho, S.P., Takahashi, M., and Yoden, S.: Indications of a strong dynamical coupling between the polar and tropical regions during the sudden stratospheric warming event January 2009, based on COSMIC/FORMASAT-3 satellite temperature data, *Atmos. Res.*, 166, 60–69, <https://doi.org/10.1016/j.atmosres.2015.06.008>, 2015.



- 515 Foelsche, U., Scherllin-Pirscher, B., Ladstätter, F., Steiner, A.K., and G. Kirchengast.: Refractivity and temperature climate records from multiple radio occultation satellites consistent within 0.05%, *Atmos. Meas. Tech.*, 4, 2007–2018, <https://doi.org/10.5194/amt-4-2007-2011>, 2011.
- Forster, P., Storelvmo, T., Armour, K., Collins, W., Dufresne, J.-L., Frame, D., Lunt, D.J., Mauritsen, T., Palmer, M.D., Watanabe, M., Wild, M., and Zhang, H.: The Earth’s energy budget, climate feedbacks, and climate sensitivity (Chapter 520 7). In *Climate Change 2021: The Physical Science Basis. Contribution of Working Group I to the Sixth Assessment Report of the Intergovernmental Panel on Climate Change*, edited by Masson-Delmotte, V., Zhai, P., Pirani, A., Connors, S.L., Pean, S. Berger, N. Caud, Y. Chen, L. Goldfarb, M.I. Gomis, M. Huang, K. Leitzell, E. Lonnoy, J.B.R. Matthews, T.K. Maycock, C., Waterfield, T., Yelekci, O., Yu, R., and Zhou, B., Cambridge University Press, Cambridge, United Kingdom and New York, NY, USA, pp. 923–1054, <https://doi.org/10.1017/9781009157896.009>, 525 2021.
- Gerber, E. P., Baldwin, M. P., Akiyoshi, H., Austin, J., and Dan, S.: Stratosphere-troposphere coupling and annular mode variability in chemistry-climate models, *J. Geophys. Res.*, 115, D00M06, <https://doi.org/10.1029/2009JD013770>, 2010.
- Gobiet, A., Kirchengast, G., Manney, G. L., Borsche, M., Retscher, C., and Stiller, G.: Retrieval of temperature profiles from CHAMP for climate monitoring: intercomparison with Envisat MIPAS and GOMOS and different atmospheric 530 analyses, *Atmos. Chem. Phys.*, 7, 3519–3536, <https://doi.org/10.5194/acp-7-3519-2007>, 2007.
- Hall, R. J., Mitchell, D. M., Seviour, W. J. M., and Wright, C. J.: Tracking the stratosphere-to-surface impact of Sudden Stratospheric Warmings, *J. Geophys. Res. Atmos.*, 126, <https://doi.org/10.1029/2020JD033881>, 2021.
- Hersbach, H., Bell, B., Berrisford, P., Hirahara, S., Horányi, A., Muñoz-Sabater, J., Nicolas, J., Peubey, C., Radu, R., Schepers, D., Simmons, A., Soci, C., Abdalla, S., Abellan, X., Balsamo, G., Bechtold, P., Biavati, G., Bidlot, J., 535 Bonavita, M., De Chiara, G., Dahlgren, P., Dee, D., Diamantakis, M., Dragani, R., Flemming, J., Forbes, R., Fuentes, M., Geer, A., Haimberger, L., Healy, S., Hogan, R.J., Hólm, E., Janisková, M., Keeley, S., Laloyaux, P., Lopez, P., Radnoti, G., De Rosnay, P., Rozum, I., Vamborg, F., Villaume, S., and Thépaut, J.-N.: The ERA5 Global Reanalysis, *Q. J. Roy. Meteor. Soc.*, 146, 1999–2049, <https://doi.org/10.1002/qj.3803>, 2020.
- Hersbach, H., Bell, W., Berrisford, P., Horányi, A., Muñoz-Sabater, J., Nicolas, J., Radu, R., Schepers, D., Simmons, A., Soci, C., and Dee, D.: Global reanalysis: goodbye ERA-Interim, hello ERA5, *ECMWF Newsl.*, 159, 17–24, 540 <https://doi.org/10.21957/vf291hehd7>, 2019.
- Hitchcock, P. and Simpson, I. R.: The downward influence of stratospheric sudden warmings, *J. Atmos. Sci.*, 71, 3586–3876, <https://doi.org/10.1175/JAS-D-14-0012.1>, 2014.
- Hitchcock, P. and Shepherd, T. G.: Zonal-mean dynamics of extended recoveries from stratospheric sudden warmings, *J. Atmos. Sci.*, 70, 688–707, <https://doi.org/10.1175/JAS-D-12-0111.1>, 2013. 545
- Holt, L. A., Randall, C. E., Peck, E. D., Marsh, D. R., Smith, A. K., and Harvey, V. L.: The influence of major sudden stratospheric warming and elevated stratopause events on the effects of energetic particle precipitation in WACCM, *J. Geophys. Res. Atmos.*, 118, 11,636–11,646, <https://doi.org/10.1002/2013JD020294>, 2013.



- Hu, J., Ren, R., and Xu, H.: Occurrence of winter stratospheric sudden warming events and the seasonal timing of spring
550 stratospheric final warming, *J. Atmos. Sci.*, 71(7), <https://doi.org/10.1175/JAS-D-13-0349.1> 2319–2334, 2015.
- Johnson, K. W., Miller, A. J., and M. Gelman.: Proposed indices characterizing stratospheric circulation and temperature
fields, *Mon. Wea. Rev.*, 97, 565–570, [https://doi.org/10.1175/1520-0493\(1969\)097<0565:PICSCA>2.3.CO;2](https://doi.org/10.1175/1520-0493(1969)097<0565:PICSCA>2.3.CO;2), 1969.
- Jonah, O. F., de Paula, E. R., Kherani, E. A., Dutra, S. L. G., and Paes, R. R.: Atmospheric and ionospheric response to
sudden stratospheric warming of January 2013, *J. Geophys. Res. Space Physics*, 119, 4973–4980,
555 <https://doi.org/10.1002/2013JA019491>, 2014.
- Kakoti, G., Kalita, B. R., Bhuyan, P. K., Baruah, S., and Wang, K.: Longitudinal and interhemispheric ionospheric response
to 2009 and 2013 SSW events in the African-European and Indian-East Asian sectors, *J. Geophys. Res. Space Physics.*,
125, <https://doi.org/10.1029/2020JA028570>, 2020
- Kirchengast, G.: Occultations for probing atmosphere and climate: Setting the scene, in: *Occultations for Probing
560 Atmosphere and Climate*, edited by: Kirchengast, G., Foelsche, U., and Steiner, A.K., 1–8, Springer, Berlin-Heidelberg,
https://doi.org/10.1007/978-3-662-09041-1_1, 2004.
- Klingler, R.: *Observing Sudden Stratospheric Warmings with Radio Occultation Data, with Focus on the Event 2009*, MSc
Thesis, 85 pp., University of Graz, Graz, Austria, URN <https://resolver.obvsg.at/urn:nbn:at:at-ubg:1-68069>, 2014.
- Kretschmer, M., Coumou, D., Agel, L., Barlow, M., Tziperman, E., and Cohen, J.: More-persistent weak stratospheric polar
565 vortex states linked to cold extremes, *Bull. Amer. Meteorol. Soc.*, 99, 49–60, <https://doi.org/10.1175/BAMS-D-16-0259.1>, 2018a.
- Kretschmer, M., Cohen, J., Matthias, V., Runge, J., and Coumou, D.: The different stratospheric influence on cold-extremes
in Eurasia and North America, *Clim. Atmos. Sci.*, 1, 44, <https://doi.org/10.1038/s41612-018-0054-4>, 2018b.
- Kursinski, E. R., Hajj, G. A., Schofield, J. T., Linfield, R. P., and Hardy, K. R.: Observing Earth’s atmosphere with radio
570 occultation measurements using the Global Positioning System, *J. Geophys. Res.*, 102, 23429–23465,
<https://doi.org/10.1029/97JD01569>, 1997.
- Kuttippurath, J. and Nikulin, G.: A comparative study of the major sudden stratospheric warmings in the Arctic winters
2003/2004–2009/2010, *Atmos. Chem. Phys.*, 12, 8115–8129, <https://doi.org/10.5194/acp-12-8115-2012>, 2012.
- Labitzke, K.: Stratospheric-mesospheric midwinter disturbances: A summary of observed characteristics, *J. Geophys. Res.*,
575 86, 9665–9678, <https://doi.org/10.1029/JC086iC10p09665>, 1981.
- Labitzke, K. and Kunze, M.: On the remarkable Arctic winter in 2008/2009, *J. Geophys. Res. Atmos.*, 114, D00I02,
<https://doi.org/10.1029/2009JD012273>, 2009.
- Ladstätter, F., Steiner, A. K., Schwärz, M., and Kirchengast, G.: Climate intercomparison of GPS radio occultation,
RS90/92 radiosondes and GRUAN from 2002 to 2013, *Atmos. Meas. Tech.*, 8, 4, 1819–1834,
580 <https://doi.org/10.5194/amt-8-1819-2015>, 2015.
- Lehtonen, I. and Karpechko, A. Yu.: Observed and modeled tropospheric cold anomalies associated with sudden
stratospheric warmings, *J. Geophys. Res. Atmos.*, 121, 1591–1610, <https://doi.org/10.1002/2015JD023860>, 2016.



- 585 Lin, J. T., Lin, C.H., Chang, L.C., Huang, H.H., Liu, J.Y., Chen, A. B., Chen, C.H., and Liu, C.H.: Observational evidence of ionospheric migrating tide modification during the 2009 stratospheric sudden warming, *Geophys. Res. Lett.*, 39, L02101, <https://doi.org/10.1029/2011GL050248>, 2012.
- Li, Y., Kirchengast, G., Schwaerz, M., Ladstätter, F., and Yuan, Y.-B.: Monitoring Sudden Stratospheric Warmings using radio occultation: a new approach demonstrated based on the 2009 event, *Atmos. Meas. Tech.*, 14, 2327-2343, <https://doi.org/10.5194/amt-14-2327-2021>, 2021.
- 590 Loeb, N.G., Mayer, M., Kato, S., Fasullo, J.T., Zuo, H., Senan, R., Lyman, J.M., Johnson, G.C., and Balmaseda, M.: Evaluating Twenty-Year Trends in Earth's Energy Flows From observations, *Earth. Space. Sci.*, <https://doi.org/10.1002/essoar.10510650.1>, 2022.
- Luntama, J.-P., Kirchengast, G., Borsche, M., Foelsche, U., Steiner, A., Healy, S., von Engel, A., O'Clérigh, E., and Marquardt, C.: Prospects of the EPS GRAS mission for operational atmospheric applications, *B. Am. Meteorol. Soc.*, 89, 1863–1875, <https://doi.org/10.1175/2008BAMS2399.1>, 2008.
- 595 Manney, G. L., Lawrence, Z. D., Santee, M. L., Read, W. G., Livesey, N. J., Lambert, A., Froidevaux, L., Pumphrey, H. C., and Schwartz M. J.: A minor sudden stratospheric warming with a major impact: Transport and polar processing in the 2014/2015 Arctic winter, *Geophys. Res. Lett.*, 42, 7808–7816, <https://doi.org/10.1002/2015GL065864>, 2015.
- McInturff, R. M.: Stratospheric warmings: Synoptic, dynamic and general-circulation aspects, *NASA Reference Publ.*, USA, NASA-RP-1017, 174, 1978.
- 600 Mitchell, D. M., Gray, L. J., Anstey, J., Baldwin, M. P., and Charlton-Perez A. J.: The influence of stratospheric vortex displacements and splits on surface climate, *J. Climate*, 26, 2668–2682, <https://doi.org/10.1175/JCLI-D-12-00030.1>, 2013.
- Nayak, C. and Yigit, E.: Variation of small-scale gravity wave activity in the ionosphere during the major sudden stratospheric warming event of 2009, *J. Geophys. Res. Space Physics.*, 124, 470–488, <https://doi.org/10.1029/2018JA026048>, 2019.
- 605 Noguchi, S., Kuroda, Y., Mukougawa, H., Mizuta, R., and Kobayashi, C.: Impact of satellite observations on forecasting sudden stratospheric warmings, *Geophys. Res. Lett.*, 47, <https://doi.org/10.1029/2019GL086233>, 2020.
- Parker, W. S.: Reanalyses and observations: What's the difference, *Bull. Amer. Meteor. Soc.*, 97, 1565–1572, <https://doi.org/10.1175/BAMS-D-14-00226.1>, 2016.
- Santer, B. D., Wigley, T., Boyle, J. S., Gaffen, D. J., Hnilo, J. J., and Nychka, D.: Statistical significance of trends and trend differences in layer-average atmospheric temperature time series, *J. Geophys. Res.*, 105, 7337-7356, <https://doi.org/10.1029/1999jd901105>, 2000.
- Scherhag, R.: Die explosionsartige Stratosphärenwärmung des Spätwinters 1951/52, *Ber. Deut. Wetterdienst*, 38, 51–63, 1952.
- 615 Scherllin-Pirscher, B., Kirchengast, G., Steiner, A. K., Kuo, Y.-H., and Foelsche, U.: Quantifying uncertainty in climatological fields from GPS radio occultation: an empirical-analytical error model, *Atmos. Meas. Tech.*, 4, 2019–2034, <https://doi.org/10.5194/amt-4-2019-2011>, 2011a.



- Scherllin-Pirscher, B., Steiner, A. K., Kirchengast, G., Kuo, Y.-H., and Foelsche, U.: Empirical analysis and modelling of errors of atmospheric profiles from GPS radio occultation, *Atmos. Meas. Tech.*, 4, 1875–1890, doi:10.5194/amt-4-1875-2011, 2011b.
- 620 Scherllin-Pirscher, B., Steiner, A. K., Kirchengast, G., Schwarzer, M., and Leroy, S. S.: The power of vertical geolocation of atmospheric profiles from GNSS radio occultation, *J. Geophys. Res.-Atmos.*, 122, 1595–1616, <https://doi.org/10.1002/2016JD025902>, 2017.
- Schoeberl, M. R.: Stratospheric warmings: Observations and theory, *Rev. Geophys.*, 16, 521–538, <https://doi.org/10.1029/RG016i004p00521>, 1978.
- 625 Schreiner, W., Rocken, C., Sokolovskiy, S., Syndergaard, S., and Hunt, D.: Estimates of the precision of GPS radio occultations from the COSMIC/FORMOSAT-3 mission, *Geophys. Res. Lett.*, 34, L04808, <https://doi.org/10.1029/2006GL027557>, 2007.
- Schwarz, M., Kirchengast, G., Scherllin-Pirscher, B., Schwarz, J., Ladstätter, F., and Angerer, B.: Multi-mission validation by satellite radio occultation extension project–Final report, Tech. Rep. for ESA/ESRIN No. 01/2016, Wegener Center, University of Graz, Graz, Austria, available at: https://wegcwww.uni-graz.at/publ/wegcpubl/arsclisys/2016/Schwarz-etal_MMValRO-FinRep_Dec2016.pdf (last access: 12 Dec 2021), 2016
- 630 Seviour, W. J. M., Mitchell, D. M., and Gray, L.J.: A practical method to identify displaced and split stratospheric polar vortex events, *Geophys. Res. Lett.*, 40, 5268–5273, <https://doi.org/10.1002/grl.50927>, 2013.
- Simmons, A., Soci, C., Nicolas, J., Bell, B., Berrisford, P., Dragani, R., Flemming, J., Haimberger, L., Healy, S., Hersbach, H., Horányi, A., Inness, A., Muñoz-Sabater, J., Radu, R., and Schepers, D.: Global stratospheric temperature bias and other stratospheric aspects of ERA5 and ERA5.1, *ECMWF Tech. Memo.*, No. 859, <https://doi.org/10.21957/rcxqfmg0>, 2020.
- Singh, R. P. and Pallamraju, D.: On the latitudinal distribution of mesospheric temperatures during sudden stratospheric warming events, *J. Geophys. Res. Space Physics.*, 120, 2926–2939, <https://doi.org/10.1002/2014JA020355>, 2015.
- 640 Siskind, D. E., Eckermann, S. D., McCormack, J. P., Coy, L., Hoppel, K. W., and Baker, N. L.: Case studies of the mesospheric response to recent minor, major, and extended stratospheric warmings, *J. Geophys. Res.*, 115, D00N03, <https://doi.org/10.1029/2010JD014114>, 2010.
- Steiner, A.K., Lackner, B.C., Ladstätter, F., Scherllin-Pirscher, B., Foelsche, U., and Kirchengast, G.: GPS radio occultation for climate monitoring and change detection, *Radio Sci.*, 46, RS0D24, <https://doi.org/10.1029/2010RS004614>, 2011.
- 645 Steiner, A. K., Ladstätter, F., Ao, C. O., Gleisner, H., Ho, S.-P., Hunt, D., Schmidt, T., Foelsche, U., Kirchengast, G., Kuo, Y.-H., Lauritsen, K. B., Mannucci, A. J., Nielsen, J. K., Schreiner, W., Schwarz, M., Sokolovskiy, S., Syndergaard, S., and Wickert, J.: Consistency and structural uncertainty of multi-mission GPS radio occultation records, *Atmos. Meas. Tech.*, 13, <https://doi.org/10.5194/amt-13-2547-2020>, 2020a.
- Steiner, A. K., Ladstätter, F., Randel, W. J., Maycock, A. C., Fu, Q., Claud, C., Gleisner, H., Haimberger, L., Ho, S.-P., 650 Keckhut, P., Leblanc, T., Mears, C., Polvani, L. M., Santer, B. D., Schmidt, T., Sofieva, V., Wing, R., and Zou, C.-



- Z.: Observed temperature changes in the troposphere and stratosphere from 1979 to 2018, *J. Climate.*, 33, 8165–8194, <https://doi.org/202010.1175/JCLI-D-19-0998.1>, 2020b.
- Stocker, M., Ladstädter, F., and Steiner, A. K.: Observing the climate impact of large wildfires on stratospheric temperature *Sci. Rep.*, 11, 22994, <https://doi.org/10.1038/s41598-021-02335-7>, 2021.
- 655 Sun, Y., Bai, W., Liu, C., Liu, Y., Du, Q., Wang, X., Yang, G., Liao, M., Yang, Z., Zhang, X., Meng, X., Zhao, D., Xia, J., Cai, Y., and Kirchengast, G.: The FengYun-3C radio occultation sounder GNOS: a review of the mission and its early results and science applications, *Atmos. Meas. Tech.*, 11, 5797–5811, <https://doi.org/10.5194/amt-11-5797-2018>, 2018.
- Thompson, D. W. J., Baldwin, M. P., and Wallace, J. M.: Stratospheric connection to northern hemisphere wintertime weather: implications for prediction, *J. Climate*, 15(12), 1421–1428, [https://doi.org/10.1175/1520-0442\(2002\)015<1421:SCTNHW>2.0.CO;2](https://doi.org/10.1175/1520-0442(2002)015<1421:SCTNHW>2.0.CO;2), 2002.
- 660 Tyrlis, E., Manzini, E., Bader, J., Ukita, J., Nakamura, H., and Matei, D.: Ural blocking driving extreme Arctic sea ice loss, cold Eurasia, and stratospheric vortex weakening in autumn and early winter 2016–2017, *J. Geophys. Res.-Atmos.*, 124, <https://doi.org/10.1029/2019JD031085>, 2019.
- Vignon E. and Mitchell D.M.: The stratopause evolution during different types of sudden stratospheric warming event, *Clim Dyn*, 44, 3323–3337, <https://doi.org/10.1007/s00382-014-2292-4>, 2015.
- 665 Van Loon, H., Jenne, R. L., and Labitzke, K.: Zonal harmonic standing waves. *J. Geophys. Res.*, 78, 4463–4471, <https://doi.org/10.1029/JC078i021p04463>, 1973.
- Wickert, J., Reigber, C., Beyerle, G., König, R., Marquardt, C., Schmidt, T., Grundwaldt, L., Galas, R., Meehan, T. K., Melbourne, W. G., and Hocke, K.: Atmosphere sounding by GPS radio occultation: First results from CHAMP, *Geophys. Res. Lett.*, 28, 32633266, <https://doi.org/10.1029/2001GL013117>, 2001.
- 670 Wickert, J., Beyerle, G., König, R., Heise, S., Grundwaldt, L., Michalak, G., Reigber, Ch., and Schmidt, T.: GPS radio occultation with CHAMP and GRACE: A first look at a new and promising satellite configuration for global atmospheric sounding, *Ann. Geophys.*, 23, 653–658, <https://doi.org/10.5194/angeo-23-653-2005>, 2005.
- WMO/IQSY.: International Years of the Quiet Sun (IQSY), 1964–1965: Alert messages with special references to stratwarms, Secretariat of the WMO WMO/IQSY Rep. 6, 19, 1964.
- 675 Yoshida, K. and Yamazaki, K.: Tropical cooling in the case of stratospheric sudden warming in January 2009: focus on the tropical tropopause layer, *Atmos. Chem. Phys.*, 11, 6325–6336, <https://doi.org/10.5194/acp-11-6325-2011>, 2011.
- Yu, Y., Ren, R., and Cai, M.: Dynamic linkage between cold air outbreaks and intensity variations of the meridional mass circulation, *J. Atmos. Sci.*, 72(8), 3214–3232, <https://doi.org/10.1175/JAS-D-14-0390.1>, 2015.
- 680 Yue, X., Schreiner, W.S., Lei, J., Rocken, C., Hunt, D.C., Kuo, Y.-H., and Wan, W.: Global ionospheric response observed by COSMIC satellites during the January 2009 stratospheric sudden warming event, *J. Geophys. Res.*, 115, A00G09, <https://doi.org/10.1029/2010JA015466>, 2010.
- Zhou, S., Miller, A.J., Wang, J., and Angell, J.K.: Downward-propagating temperature anomalies in the preconditioned polar stratosphere, *J. Climate*, 15(7), 781–792, [https://doi.org/10.1175/1520-0442\(2002\)015<0781:DPTAIT>2.0.CO;2](https://doi.org/10.1175/1520-0442(2002)015<0781:DPTAIT>2.0.CO;2), 2002.



685 **Table 1.** Basic parameters and methodology of the new SSW monitoring approach (all parameters are updated daily; the boldfaced font in (2)-(4) and (7)-(10) marks key parameters for the monitoring as also shown in Figs. 6 to 8).

Parameter	Equation/Definition	Explanation/Description
(1) Temperature anomaly profile $\Delta T_{\text{Anomaly}}$	$\Delta T_{\text{Anomaly}} = T - T_{\text{Cli}} \text{ [K]}$	T represents an individual RO or ERA5 profile, T_{Cli} is the collocated climatological profile.
(2) Middle Stratosphere Temperature Anomaly Threshold Exceedance Area: MSTA-TEA [10^6 km^2]	Altitude range: 30–35 km Thresholds selected: +50 K, +40 K, +30 K; -30 K, -40 K, -50 K	Based on individual $\Delta T_{\text{Anomaly}}$ profiles in selected stratospheric altitude layers (e.g., 30–35 km for MSTa-TEA) first estimate layer-mean anomaly values from these profiles. The individual layer-mean values are then averaged into a suitable space-time-binned grid over 50–90 °N (5 °latitude \times 20 °longitude grid). The geographic areas wherein grid-cell anomalies exceed predefined thresholds (e.g., +30 K) are finally calculated and stored as the Threshold Exceedance Area (TEAs).
(3) Lower Stratosphere Temperature Anomaly Threshold Exceedance Area: LSTA-TEA [10^6 km^2]	Altitude range: 20–25 km Thresholds selected: +30 K, +25 K, +20 K; -20 K, -25 K, -30 K	
(4) Upper Stratosphere Temperature Anomaly Threshold Exceedance Area: USTA-TEA [10^6 km^2]	Altitude range: 40–45 km Thresholds selected: +50 K, +40 K, +30 K; -30 K, -40 K, -50 K	
(5) Anomaly Maximum value	$\Delta T_{\text{AMax}} \text{ [K]}$	Maximum (positive/negative) anomaly value of all grid cells within a TEA obtained by (2)-(4)
(6) Geographic location (Lat, Lon) of Anomaly Maximum value	$\varphi^{\text{AMax}} \text{ [}^\circ\text{N]}, \lambda^{\text{AMax}} \text{ [}^\circ\text{E]}$	Generate a contour that is 2 K smaller/larger than the positive/negative ΔT_{AMax} value; the center of the contour is then used as geographic location of the ΔT_{AMax} value.
(7) SSW Primary-Phase Threshold Exceedance Area: SSW-PP-TEA [10^6 km^2]	$\text{SSW-PP-TEA} = (\text{MSTA-TEA} > +30 \text{ K})$	Expresses the main and primary stratospheric warming anomaly strength; recorded if SSW-PP-TEA > TEA_{Min} ($3 \times 10^6 \text{ km}^2$) for ≥ 3 days.
(8) SSW Secondary-Phase Threshold Exceedance Area: SSW-SP-TEA [10^6 km^2]	$\text{SSW-SP-TEA} = (\text{LSTA-TEA} > +20 \text{ K})$	Expresses the secondary downward propagated warming anomaly strength; recorded if a SSW-PP-TEA is recorded (see (7)) and if during its presence the SSW-SP-TEA emerges and then exceeds TEA_{Min} ($3 \times 10^6 \text{ km}^2$) for ≥ 5 days.
(9) SSW Main-Phase Threshold Exceedance Area: SSW-MP-TEA [10^6 km^2]	$\text{SSW-MP-TEA} = \text{Max}(\text{SSW-PP-TEA}, \text{SSW-SP-TEA})$	Expresses the combined warming of primary- and secondary phase; it takes the higher value of SSW-PP-TEA and SSW-SP-TEA at any day.
(10) SSW Trailing-Phase Threshold Exceedance Area: SSW-TP-TEA [10^6 km^2]	$\text{SSW-TP-TEA} = \text{Abs}(\text{USTA-TEA} < -30 \text{ K})$	Expresses the trailing upper stratosphere cooling anomaly strength; recorded if SSW-TP-TEA > TEA_{Min} ($3 \times 10^6 \text{ km}^2$) for ≥ 21 days.



690 **Table 2.** Metrics of the new SSW monitoring approach for detection, classification, and further qualification (the boldfaced font in (1)–(5) marks key metrics and criteria for the detection and classification also shown as main ones in Fig. 9).

Parameter	Equation/Definition	Explanation/Description
(1) Main-phase duration metric:	SSW-MPD [days]	Expresses SSW warming duration: number of days with SSW-MP-TEA available (at $> TEA_{Min}$ of $3 \times 10^6 \text{ km}^2$)
(2) Main-phase area metric:	SSW-MPA [10^6 km^2]	Expresses SSW mean warming area: average daily area of SSW-MP-TEA during all SSW-MPD days
(3) Main-phase strength metric:	SSW-MPS [$10^6 \text{ km}^2 \text{ days}$] $= (\text{SSW-MPA} \times \text{SSW-MPD})$	Express SSW warming strength: the larger this area-duration product, the stronger the event
(4) SSW detection criterion:	SSW-MPD ≥ 7 days	SSW event adopted as detected and logged to the event count
(5) SSW classification criteria:	SSW-MPS $< 90 \text{ } 10^6 \text{ km}^2 \text{ days}$	Minor SSW event
	SSW-MPS $\geq 90 \text{ } 10^6 \text{ km}^2 \text{ days}$ and $\leq 180 \text{ } 10^6 \text{ km}^2 \text{ days}$	Major SSW event
	SSW-MPS $> 180 \text{ } 10^6 \text{ km}^2 \text{ days}$	Extreme SSW event
(6) Trailing-phase duration metric:	SSW-TPD [days]	Expresses the trail-cooling duration: number of days with SSW-TP-TEA available (at $> TEA_{Min}$ of $3 \times 10^6 \text{ km}^2$)
(7) Trailing-phase area metric:	SSW-TPA [10^6 km^2]	Express the mean trail-cooling area: Average daily area of SSW-TP-TEA during all SSW-TPD days
(8) Further SSW qualification:	SSW-TPD < 21 days	Non-trail-cooling event
	SSW-TPD ≥ 21 days	Trail-cooling event (TC)
(9) SSW onset calendar date	Onset date [yyyy-mm-dd]	The day when the primary-phase exceedance area SSW-PP-TEA is largest (based on (7) in Table 1)
(10) SSW onset geographic location (latitude/longitude)	Onset location [N / E]	Location where ΔT_{AMax} occurs at the onset date (based on (6) in Table 1)
(11) SSW onset maximum warming anomaly	Max ΔT [K]	Maximum warming anomaly ΔT_{AMax} associated with the SSW-PP-TEA at onset date (based on (5) in Table 1)



Table 3. SSW climatology summary for 1979–2021 based on ERA5 (for definition and units of all parameters see Table 2).

Winters	Onset date	MPS	MPD	MPA	Type	Max ΔT	Onset location	Onset date BG18
W79-80	—	—	—	—	—	—	—	1980-02-29
W80-81	1981-02-04	88.2	9	9.8	Minor	43.7	83.6°N/46.4°E	1981-02-06
W81-82	—	—	—	—	—	—	—	1981-12-04
W82-83	1983-01-27	73.3	8	9.2	Minor	51.9	78.9°N/87.4°E	—
W83-84	1984-02-23	66.7	8	8.3	Minor	44.6	72.1°N/61.6°E	1984-02-24
W84-85	1985-01-01	192.3	16	12.0	Extreme(TC)	54.5	66.1°N/101.4°W	1985-01-01
W85-86	—	—	—	—	—	—	—	—
W86-87	1987-01-24	51.8	7	7.4	Minor	46.8	65.6°N/39.1°E	1987-01-23
W87-88	1987-12-07	211.9	18	11.8	Extreme	68.4	68.9°N/49.0°E	1987-12-08
W88-89	1989-02-12	275.2	21	13.1	Extreme	49.6	84.9°N/24.2°W	1989-02-21
	1989-02-20	49.8	7	7.1	Minor	57.6	61.2°N/60.7°W	
W89-90	1990-02-09	97.3	11	8.8	Major	61.6	70.6°N/80.3°E	—
W90-91	1991-01-09	121.8	10	12.2	Major	59.4	72.7°N/51.4°W	—
W91-92	1992-01-11	129.9	13	10.0	Major	64.7	77.6°N/71.9°E	—
W92-93	1993-02-20	33.2	7	4.7	Minor	45.2	73.3°N /72.2°E	—
W93-94	—	—	—	—	—	—	—	—
W94-95	1994-12-30	57.7	7	8.2	Minor	56.9	70.3°N/140.6°E	—
	1995-01-26	144.9	15	9.7	Major	57.3	71.4°N/70.9°E	
W95-96	—	—	—	—	—	—	—	—
W96-97	—	—	—	—	—	—	—	—
W97-98	—	—	—	—	—	—	—	—
W98-99	1998-12-14	175.8	15	11.7	Major	57.9	72.7°N/100.3°E	1998-12-15
	1999-02-23	85.1	11	7.7	Minor	53.3	77.2°N/89.2°E	1999-02-26
W99-00	—	—	—	—	—	—	—	2000-03-20
W00-01	2000-12-07	83.1	10	8.3	Minor	56.6	68.7°N/68.7°E	2001-02-11
	2000-12-18	43.9	7	6.3	Minor	39.8	69.1°N/53.9°W	
	2001-01-28	51.1	7	7.3	Minor	49.6	70.3°N/77.9°E	
W01-02	2001-12-22	224.9	21	10.7	Extreme	64.9	73.0°N/48.9°E	2001-12-31
W02-03	2002-12-28	161.6	14	11.5	Major	74.8	70.8°N/38.3°E	2003-01-18
W03-04	2003-12-24	107.6	14	7.7	Major	48.0	80.7°N/ 82.1°E	2004-01-05
	2004-01-04	120.6	15	8.0	Major (TC)	50.7	66.2°N/40.7°E	
W04-05	—	—	—	—	—	—	—	—
W05-06	2006-01-11	43.6	7	6.2	Minor	51.0	72.5°N/59.4°E	2006-01-21
	2006-01-21	114.6	12	9.5	Major (TC)	48.1	68.4°N/20.1°E	
W06-07	2007-01-01	72.4	10	7.2	Minor	43.1	84.6°N/97.5°E	2007-02-24
W07-08	2008-01-23	73.9	8	9.2	Minor	55.8	80.7°N/87.5°E	2008-02-22
	2008-02-23	68.3	8	8.5	Minor	56.9	65.7°N/18.7°E	
W08-09	2009-01-23	366.8	24	15.3	Extreme(TC)	65.9	76.8°N/48.6°W	2009-01-24
W09-10	2010-01-29	68.5	8	8.6	Minor	58.8	68.3°N/59.7°E	2010-02-09
W10-11	—	—	—	—	—	—	—	—
W11-12	2012-01-17	112.1	12	9.3	Major	55.2	72.5°N/42.6°E	—
W12-13	2013-01-05	191.2	22	8.7	Extreme(TC)	48.5	67.9°N/62.5°E	2013-01-07
W13-14	2014-02-08	100.4	11	9.1	Major	69.1	70.1°N/39.4°W	—
W14-15	2015-01-06	146.5	16	9.2	Major	54.9	70.2°N/30.9°W	—
W15-16	2016-03-05	74.9	9	8.3	Minor	51.1	77.8°N/59.2°E	—
W16-17	2017-01-28	59.4	10	5.9	Minor	56.8	75.8°N/88.9°E	—
W17-18	2018-02-16	207.5	18	11.5	Extreme	60.9	61.8°N/102.0°W	—
W18-19	2018-12-25	290.8	31	9.4	Extreme(TC)	60.2	77.9°N/72.5°E	—
W19-20	2020-03-21	57.1	7	8.2	Minor	41.7	86.5°N/22.8°E	—
W20-21	2021-01-03	110.2	11	10.0	Major	55.8	75.7°N/11.2°E	—



700 **Table 4.** SSW climatology summary 2006-2020 based on RO, for main metrics, for enabling quantitative intercomparison to the results based on ERA5 as summarized in Table 3 (for definition and units of the parameters see Table 2).

Winters	Onset date	MPS	MPD	MPA	Winters	Onset date	MPS	MPD	MPA
W06-07	2007-01-01	49.7	7	7.1	W13-14	2014-02-08	84.0	10	8.4
W07-08	—	—	—	—	W14-15	2015-01-06	128.8	16	8.0
W08-09	2009-01-22	329.7	22	15.0	W15-16	2016-03-05	70.1	9	7.8
W09-10	2010-01-29	56.3	7	8.0	W16-17	2017-01-28	52.2	9	5.8
W10-11	—	—	—	—	W17-18	2018-02-15	186.0	17	10.9
W11-12	2012-01-17	98.2	11	8.9	W18-19	2018-12-25	275.3	30	9.2
W12-13	2013-01-05	164.5	21	7.8	W19-20	—	—	—	—

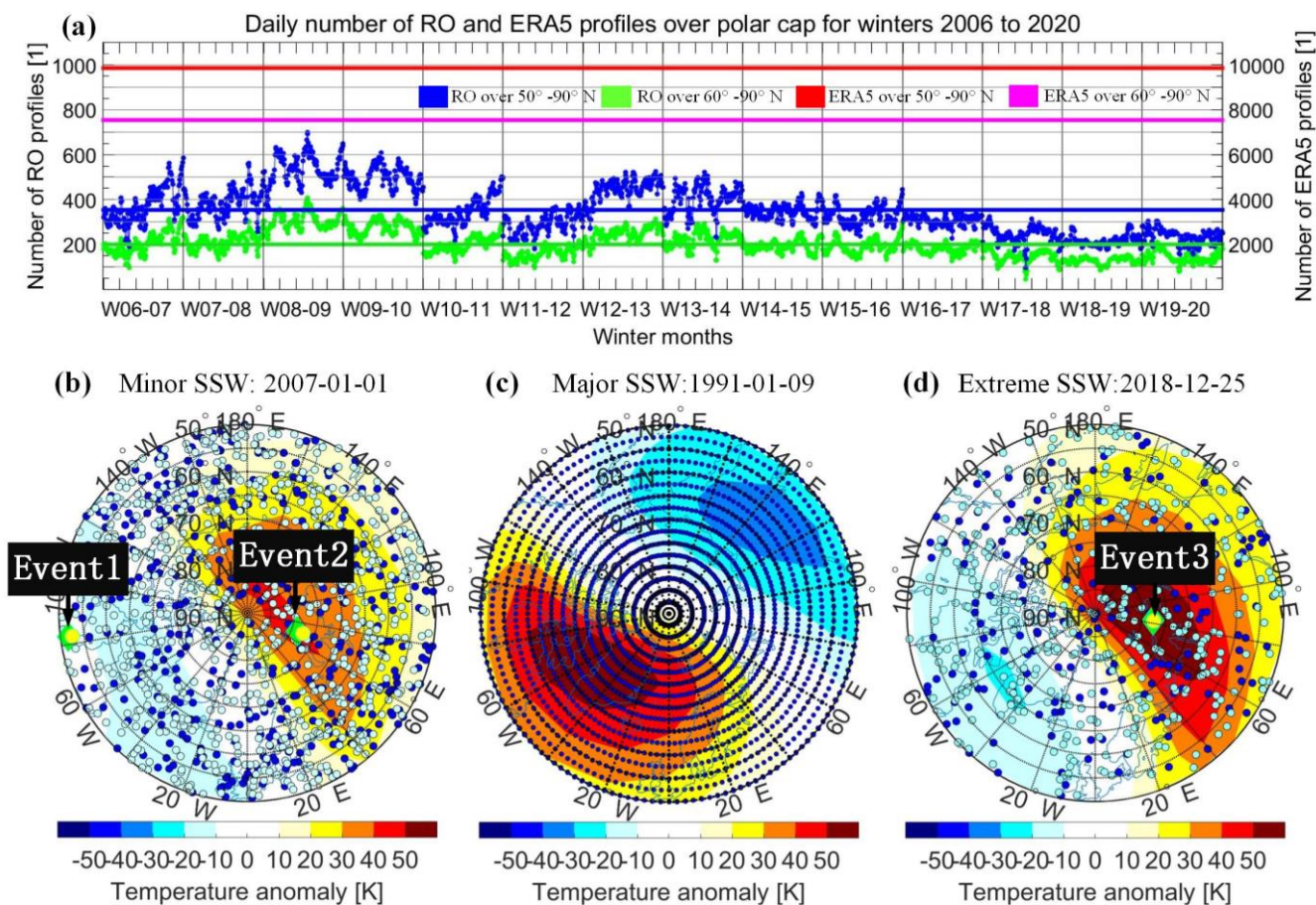


Figure 1. Number and distribution of RO and ERA5 profile data over the Northern polar region. **(a):** Daily number of RO events over 50-90° N (blue dots) and 60-90° N (green dots) for 14 winters from W06-07 to W19-20, with the blue and green horizontal lines showing the related long-term average number, as well as the (constant) daily number of ERA5 grid-point profiles (red and magenta lines); **(b):** illustrative distribution of RO event locations on 01 Jan 2007 (blue dots), and on the previous and next days (light blue dots), over-plotted on the middle-stratosphere temperature anomaly (MSTA) of the day (color bar), on which a minor SSW prevailed; **(c):** distribution of the regular ERA5 grid-point profile locations (2.5° latitude × 2.5° longitude grid), over-plotted on the MSTAs of 09 Jan 1991, where a major SSW prevailed; **(d):** illustrative distribution of RO event locations on 25 Dec 2018 in the same style as in (b), over-plotted on the MSTAs of the day, on which an extreme SSW prevailed. The green diamonds / yellow circles in (b) and (d) show the location of three exemplary RO events / ERA5 profiles (Event1 to Event3) that are located in different SSW anomaly strength conditions and used in Fig. 2 to illustrate the anomalies construction concept.

715

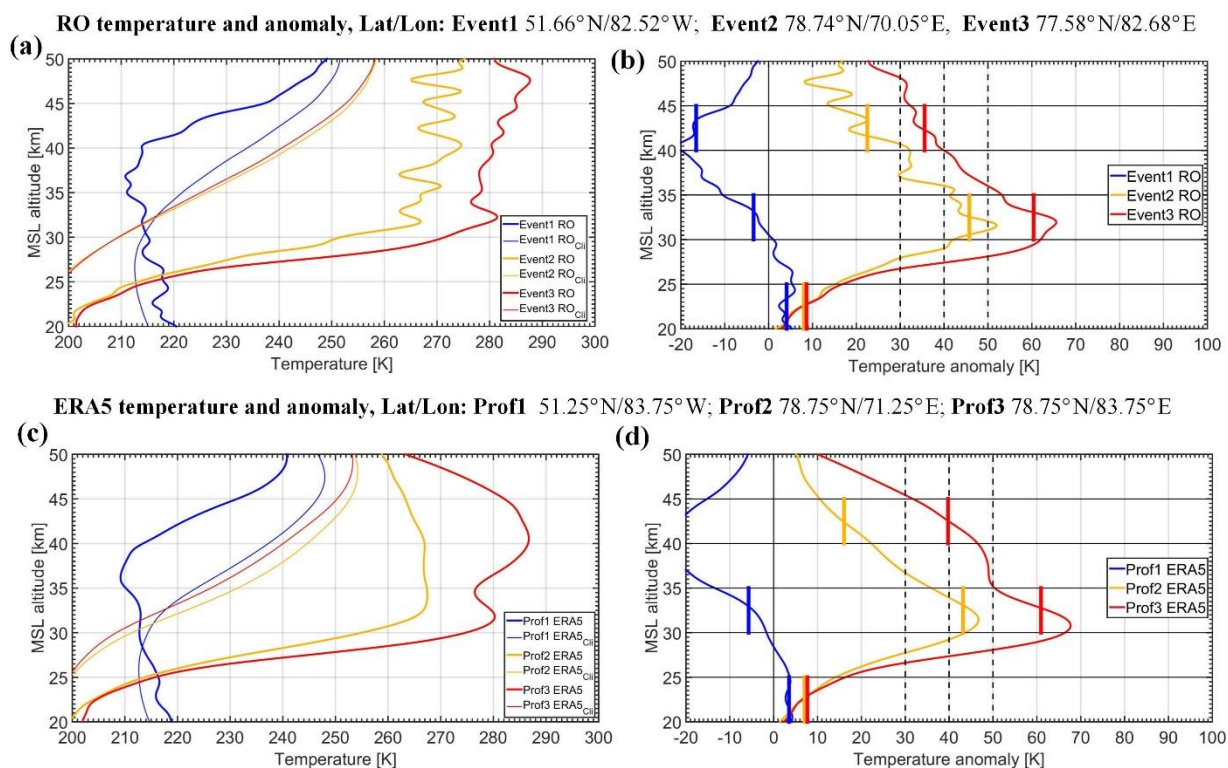
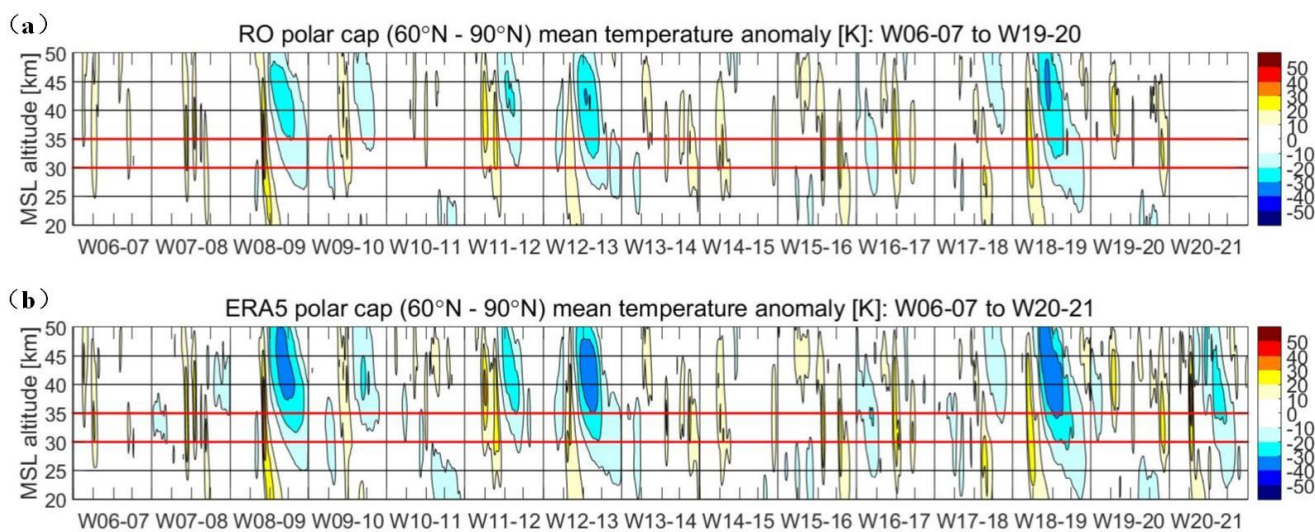
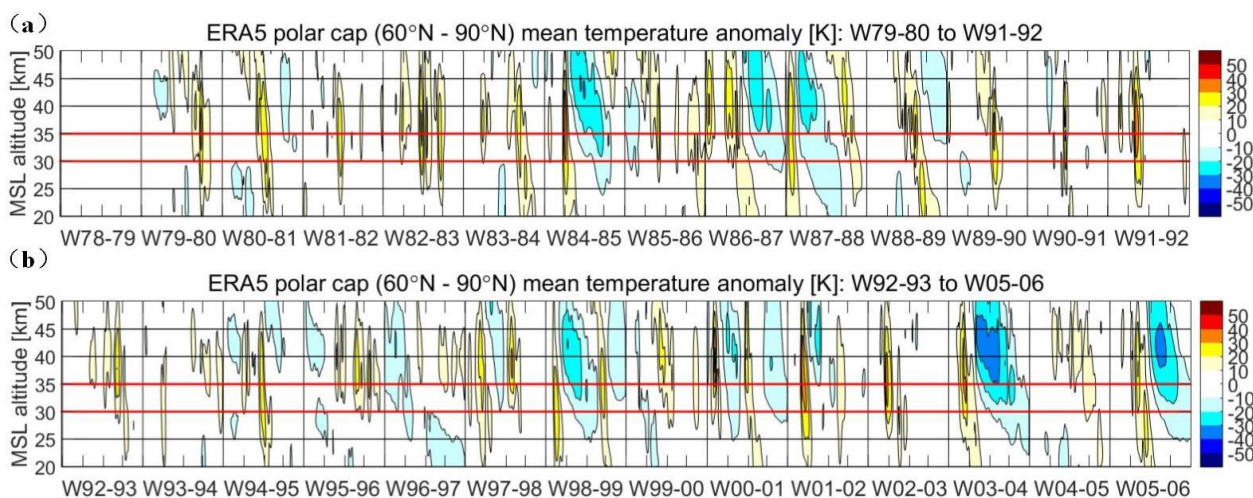


Figure 2. Illustration of anomaly construction, layer selection, and computation of layer-mean anomaly values based on the three example RO events / ERA5 profiles indicated in Fig. 1b, d. (a): Event 1 to 3 temperature profiles from RO and collocated climatological profiles RO_{Cli}; (b): RO temperature anomaly profiles from the difference of RO to RO_{Cli} profiles as well as indication of the lower-stratosphere (20-25 km), middle stratosphere (30-35 km), and upper stratosphere (40-45 km) layers and associated layer-mean anomaly values; (c): Profile 1 to 3 temperature and corresponding climatological profiles from ERA5 in same style as (a); (d): ERA5 temperature anomaly profiles and layer-mean values in the same style as (b). The RO satellites and event times, and ERA5 analysis time layers, of these examples are (for the locations see the panel headers): Event1: COSMIC-FM1 event 01 Jan 2007 04:28 UTC; Event2: COSMIC-FM1 event 01 Jan 2007 22:44 UTC; Event3: MetOp-A event 25 Dec 2018 17:04 UTC; Prof1: ERA5 profile 01 Jan 2007 06:00 UTC; Prof2: ERA5 profile 02 Jan 2007 00:00 UTC; Prof3: ERA5 profile 25 Dec 2018 18:00 UTC. The climatological profiles are extracted (and interpolated to the needed locations and times) from long term-averaged (2006-2020 for RO and 1979-2020 for ERA5) monthly mean $2.5^\circ \times 2.5^\circ$ temperature fields.



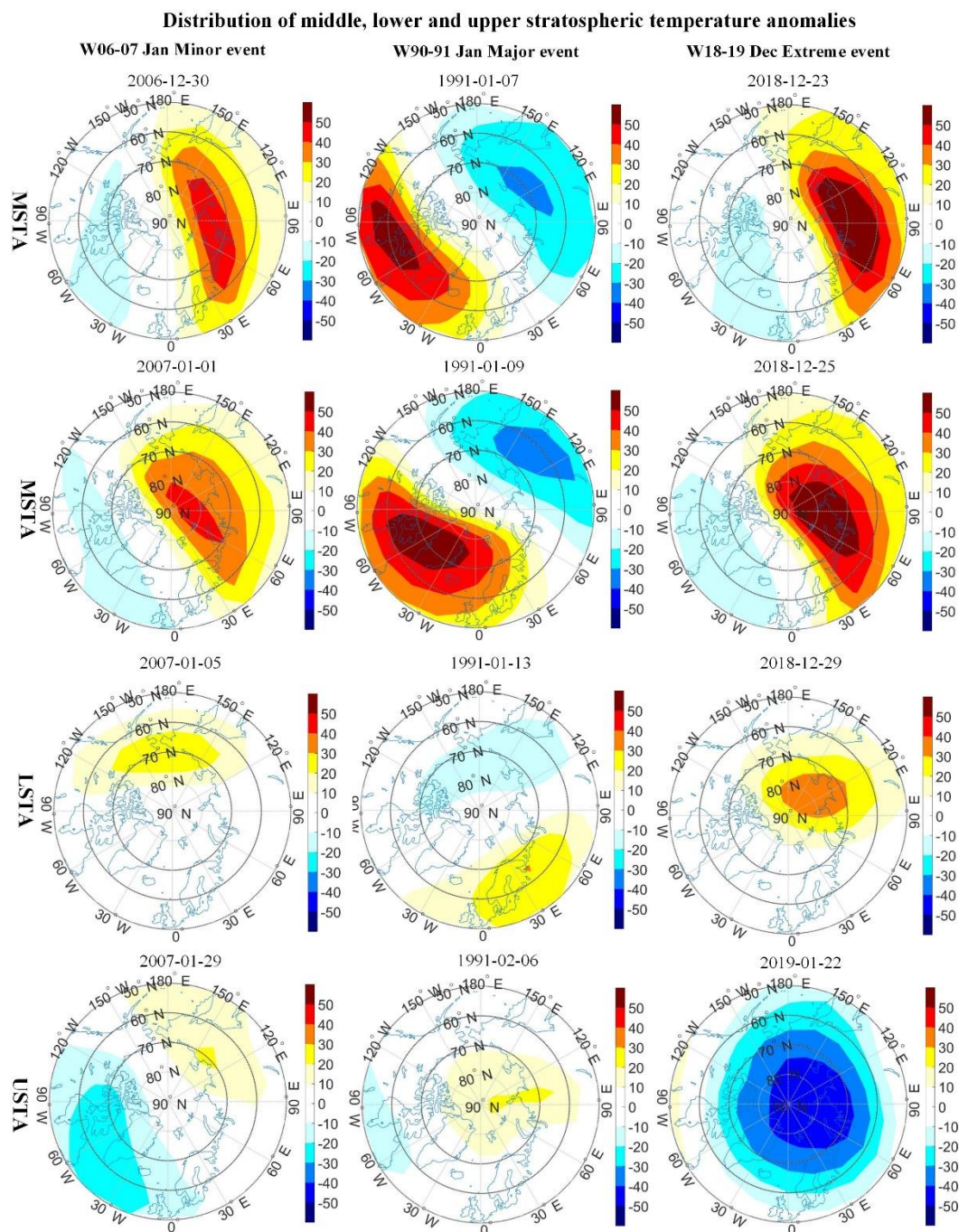
730

Figure 3. Temporal evolution of polar-cap mean (60° - 90° N) daily mean temperature anomaly profiles from RO (a) and ERA5 (b), over four winter months each (December, January, February, March), for the winters from 2006-07 (W06-07) to 2019-20 for RO (W19-20) and 2020-21 for ERA5 (W20-21). The RO dataset did not yet cover the W20-21 time period.



735

Figure 4. Temporal evolution of polar-cap mean (60° - 90° N) daily mean temperature anomaly profiles from ERA5, over four winter months each (December, January, February, March), for the winters from W79-80 to W91-92 (a) and from W92-93 to W05-06 (b), respectively. The W78-79 time period was not covered by the ERA5 dataset used.



740

Figure 5. Polar-view (50 °90 °N) contour maps of W06-07 Jan Minor (left), W90-91 Jan Major (middle) and W18-19 Dec Extreme (right) SSW example events (cf. Figs. 1 and 6), illustrating ERA5-based Middle Stratosphere Temperature Anomalies (MSTA), Lower Stratosphere Temperature Anomalies (LSTA), and Upper Stratosphere Temperature Anomalies (USTA). MSTA (top and second row) is shown two days before and on the defined onset date (see Table 2 for definition), LSTA (third row) 4 days after the onset date, and USTA (bottom) 4 weeks after the onset date, respectively.

745

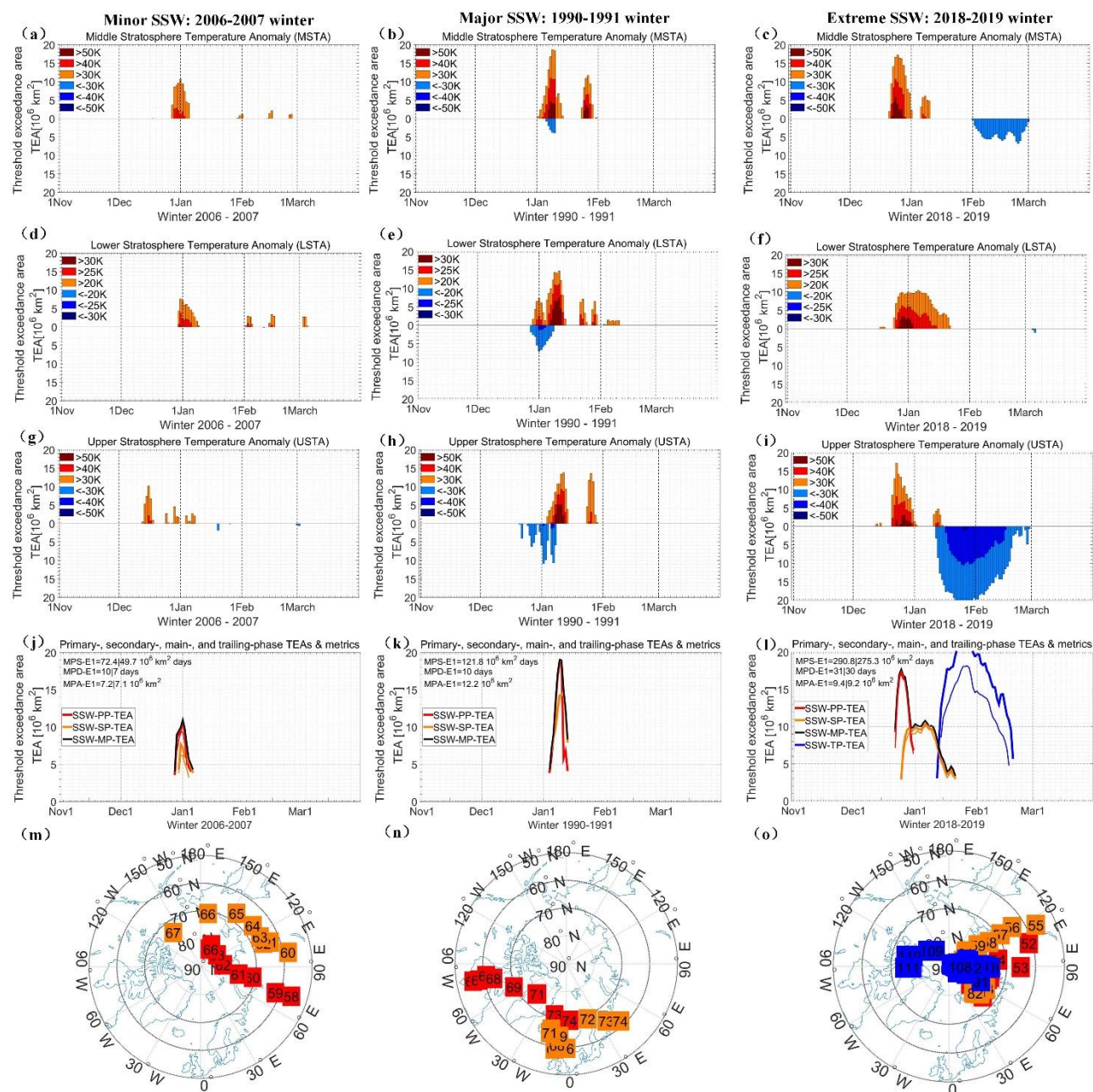
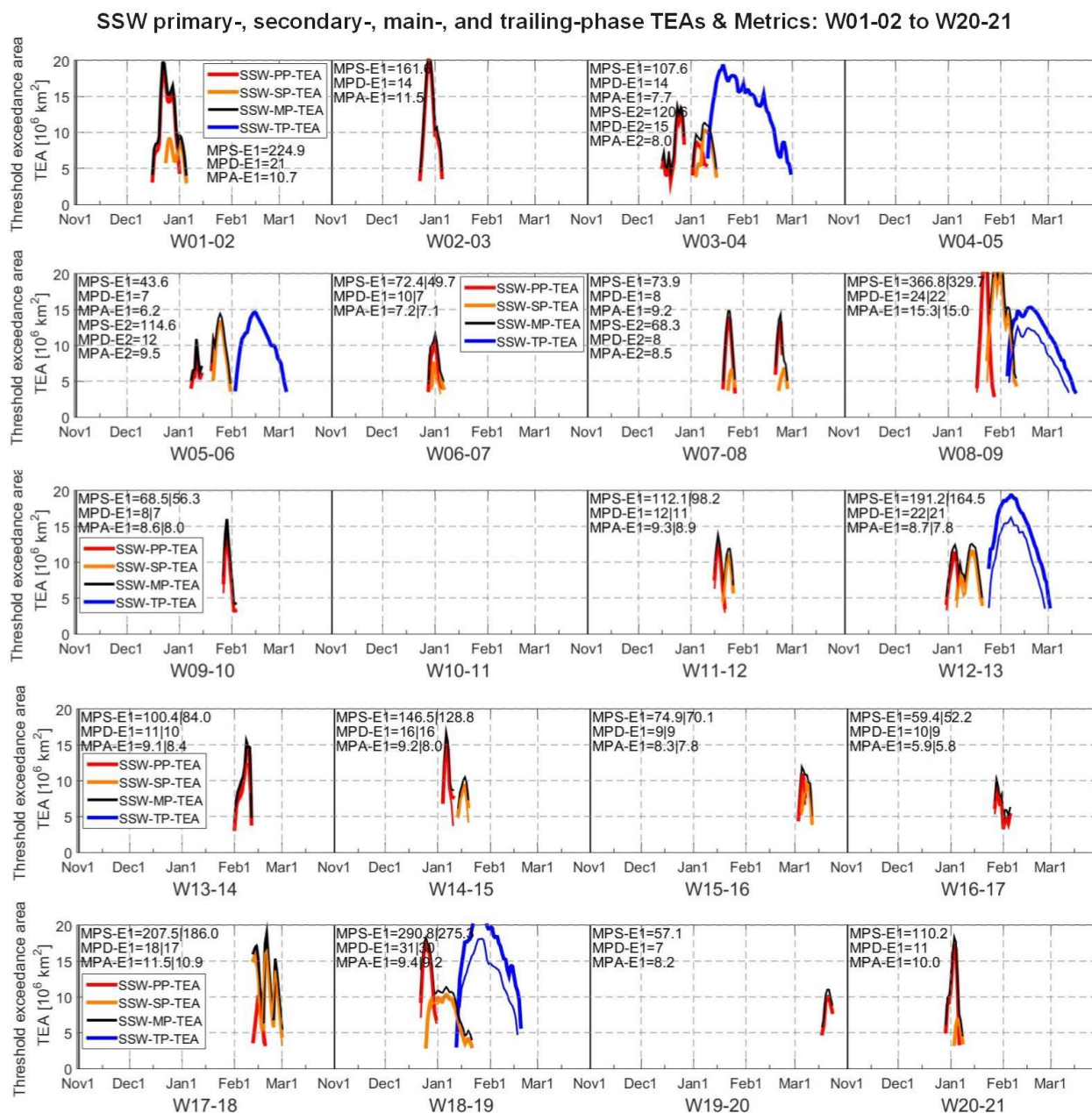
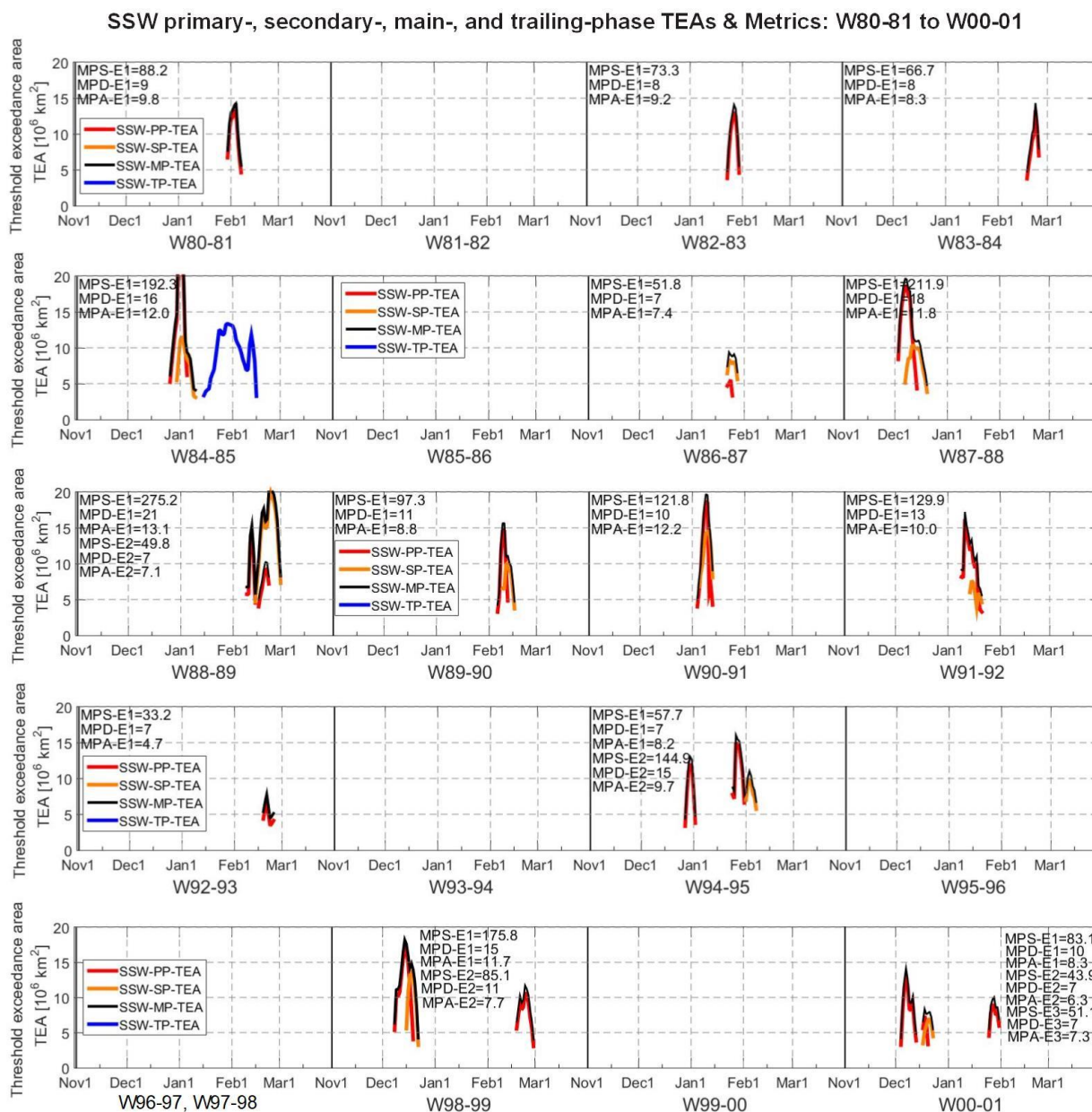


Figure 6. Time evolution of the daily ERA5 MSTA (a, b, c), LSTA (d, e, f) and USTA (g, h, i) Threshold Exceedance Areas (TEAs) for the same Minor (left), Major (middle) and Extreme (right) SSW events as illustrated in Fig. 5. Panels (j), (k), and (l) depict the four derived SSW TEAs (SSW-PP-TEA, SSW-SP-TEA, SSW-MP-TEA, and SSW-TP-TEA in case it occurs) according to Table 1, (7)-(10); the SSW metrics MPS, MPD, and MPA (see Table 2) are also noted in each panel, and heavy and light lines denote ERA5 and RO results, respectively (difference especially visible for the extreme event). Panels (m), (n), and (o) illustrate geographical tracks (numbered by day-of-winter as of 1st Nov) of maximum positive/negative anomaly values of SSW-PP-TEA (red), SSW-SP-TEA (orange) and SSW-TP-TEA (blue).

750



755 **Figure 7.** Time evolution of the SSW TEAs (SSW-PP-TEA, SSW-SP-TEA, SSW-MP-TEA, SSW-TP-TEA as applicable; definitions see Table 1) for all recorded SSW events of the winters W01-02 to W20-21; the SSW metrics MPS, MPD, and MPA (definitions and units see Table 2) are noted in the panels (E1, E2 are SSW event numbers, ordered according to the occurrence time in a winter). ERA5 results (heavy lines) are complemented by RO results (light lines, especially visible for stronger events) for the winters W06-07 to W19-20.



760

Figure 8. Time evolution of the SSW TEAs (SSW-PP-TEA, SSW-SP-TEA, SSW-MP-TEA, SSW-TP-TEA) and related SSW metrics (MPS, MPD, MPA) for all recorded SSW events of the winters W80-81 to W00-01; same plotting style as Fig. 7.

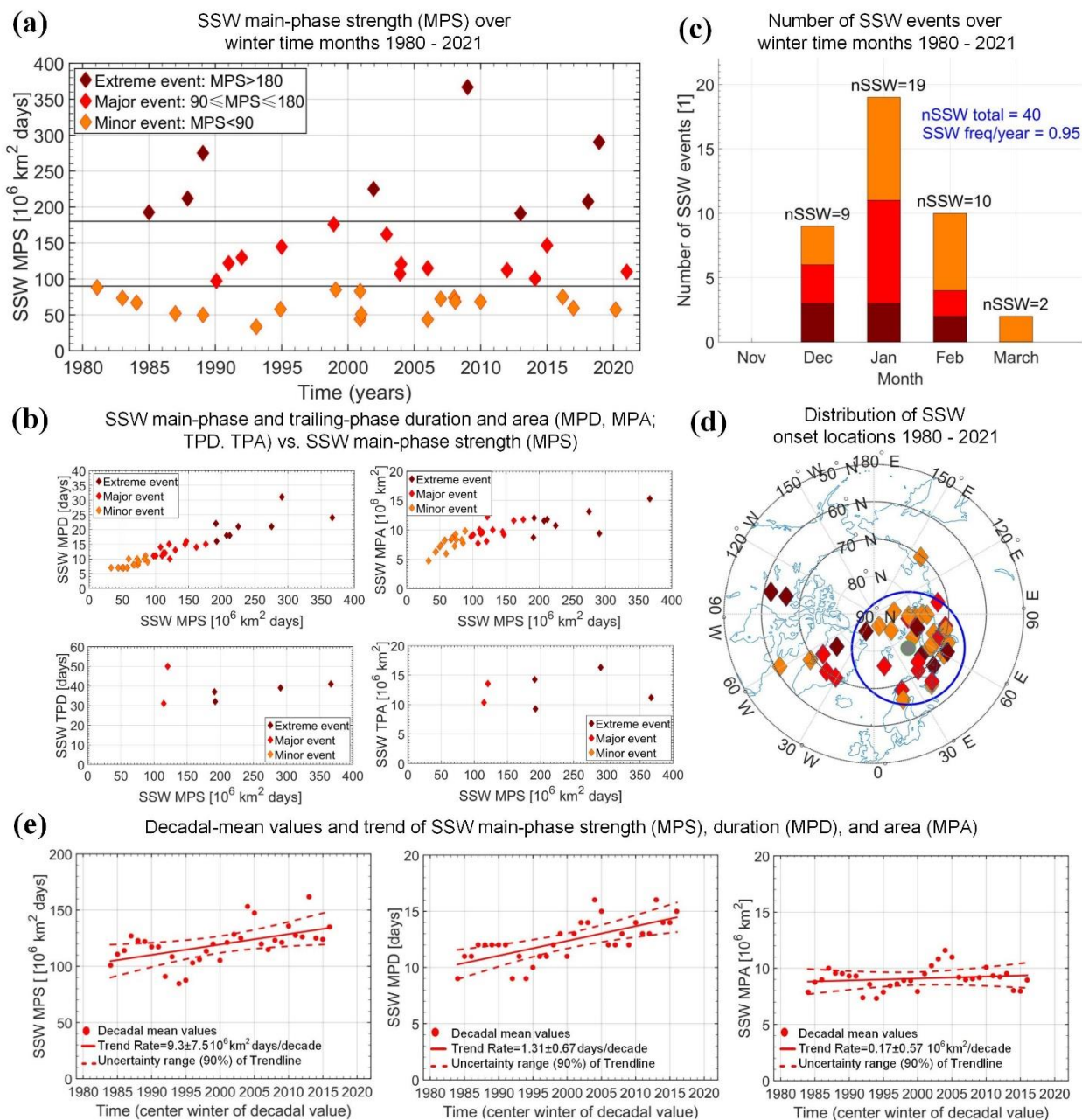


Figure 9. Overview of main characteristics of the 40 SSW events recorded over the 42 winters from 1980 to 2021 based on ERA5 data using the new monitoring approach (see Table 3 for a tabular summary). **(a):** time evolution of main-phase strengths (MPS) (year tick marks denote January-of-year); **(b):** relation of main-phase and trailing-phase duration and area (MPD, MPA; TPD, TPA) to main-phase strength (MPS); **(c):** distribution of the number of events over the winter months (showing the three strength types by the same color as in a, b); **(d):** spatial distribution of onset locations, indicating the clustering of more than 75% of the events over the Northern Eurasia/Polar ocean region by a circle (using the same strength-type colors as in a, b); **(e):** assessment of long-term trends in SSW main-phase strength, duration, and area, noting also main statistical results within the respective panels (for description see text).